https://doi.org/10.1016/j.jcsr.2019.02.022

Behavior of cold-formed steel elliptical hollow sections subjected to bending

Man-Tai Chen [a,*], Ben Young [b]

[a] *Department of Civil Engineering, The University of Hong Kong, Pokfulam Road, Hong Kong, China*

[b] *Department of Civil and Environmental Engineering, The Hong Kong Polytechnic University, Hong Kong, China (Formerly, Department of Civil Engineering, The University of Hong Kong, Pokfulam Road, Hong Kong, China)*

Abstract

This paper presents the experimental and numerical investigation on the behavior of cold-formed steel elliptical hollow section beams. In the test program, a total of 20 beam tests was conducted. Four elliptical section series with the nominal cross-section aspect ratio ranging from 1.65 to 3 were bent about the major and minor axes in both three-point and four-point bending configurations. Finite element models were established to replicate the beam tests numerically. Based upon the validated model, extensive parametric study was conducted on 235 beam specimens to study the behavior of cold-formed steel elliptical hollow sections subjected to bending. The results obtained from experimental and numerical investigation were used to assess the existing design methods and to propose modified design methods for cold-formed steel elliptical hollow section beams. It should be noted that the current design codes do not cover the design of elliptical hollow section beams. The flexural strengths of beams were compared with the design strengths predicted by the equivalent diameter and equivalent rectangular section methods proposed by previous researchers, the traditional design methods using equivalent diameter as well as the Direct Strength Method and the Continuous Strength Method. The applicability and reliability of these design methods were assessed. The results indicate that the existing design methods are not capable to predict the flexural strengths of cold-formed steel elliptical hollow section beams in accurate and reliable manner. In this study, the modified Direct Strength Method and Continuous Strength Method are proposed, which provide accurate and reliable flexural strength predictions.

Keywords: Beam; Cold-formed steel; Elliptical hollow sections; Finite element; Structural design.

---

* Corresponding author.
E-mail address: cmt111@connect.hku.hk (M.T. Chen).

1. Introduction

As a new member in the family of tubular sections, elliptical hollow section (EHS) possesses the structural attribute of different geometric properties in the major and minor axes. This allows elliptical hollow section to be orientated to resist applied load more effectively thus the EHS can offer more efficient and economic use of material than square and circular hollow sections [1, 2]. The streamlined profile of EHS is especially favorable when the structure is exposed to wind or water forces due to its lower drag coefficient compared with square and rectangular sections. In addition to its prominent structural properties, the appealing appearance of EHS provides an attractive choice to the designers and engineers. The merits of EHS underpin its potential in the engineering applications and have attracted the attention of researchers. The research group in Imperial College London has conducted a series of tests as well as theoretical and numerical analyses on the structural behavior of EHS, which have primarily focused on structural response of hot-finished steel EHS [3-11] and cold-formed stainless steel EHS [12, 13]. Based on the findings, equivalent diameter method [14] and equivalent rectangular hollow section (RHS) approach [15] have been proposed for the design strength predictions of hot-finished steel EHS structural members. Nonetheless, the investigation on cold-formed steel EHS structural members is scarce [16, 17] and the applicability of those design methods for cold-formed steel EHS subjected to bending is questionable.

The main objective of this paper is to investigate the structural behavior of cold-formed steel elliptical hollow section beams through experimental and numerical studies. A series of bending tests and an extensive numerical study with a wide range of cross-section geometries were conducted on beam specimens bent about the major and minor axes. The results obtained from tests and numerical study were used to evaluate the applicability and reliability of the existing design methods, such as the equivalent diameter method [14], the equivalent RHS approach [15], the traditional design methods [18-20] using equivalent diameter as well as the Direct Strength Method

(DSM) [18] and the Continuous Strength Method (CSM) [21-24]. Modifications are suggested for the Direct Strength Method and the Continuous Strength Method to improve the accuracy of the flexural strength predictions in a reliable manner.

2. Experimental investigation

2.1. Beam specimens

A total of 20 bending tests, including 10 four-point bending tests and 10 three-point bending tests, was conducted. The cold-formed steel EHS beams were subjected to bending about the major (z-z) axis and the minor (y-y) axis. Four series of EHS were included in the experimental program. The cross-section geometry of EHS is defined with symbols shown in Fig. 1. The nominal dimensions ($D\times B\times t$) of EHS are 140×85×3, 150×50×5, 150×70×3 and 180×65×5, where D, B and t are the larger outer diameter, the smaller outer diameter and the wall thickness of the section, respectively. The specimens are labeled so that the nominal cross-section geometry, bending configuration and bending axis can be identified. In the specimen label, the nominal cross-section geometry and a number that identifies the bending configuration is separated by a hyphen, where the number "3" and "4" mean three-point and four-point bending configurations, respectively. The following letter designates the bending axis of specimen, where "Y" and "Z" indicate beam specimen subjected to bending about the minor and major axes, respectively. The symbol of "#" in the label indicates that it is a repeated test. For example, the label 150×70×3-3Y# represents a repeated test of a specimen subjected to bending about the minor axis in three-point bending configuration with nominal cross-section dimensions of 150×70×3. The cross-section dimensions of the specimens were measured and are reported in Table 1.

The manufacturing processes of cold-formed steel EHS investigated in this study have been described in Chen and Young [17]. Tensile coupon tests were conducted to determine the material properties of the cold-formed steel EHS. Tensile coupon specimens were machined longitudinally along both flattest portion (TC1) and curviest portion (TC2) of EHS as shown in Fig. 2. The details of tensile coupon tests have been reported by Chen and Young [17], and a summary of obtained

material properties is shown in Table 2. The nominal cross-section aspect ratio of EHS (D/B) covers a wide range from 1.65 to 3. In four-point bending configuration, the moment span between the two loading points (L_m = 500mm) and the shear spans between the end supports and the adjacent loading points (L_s = 600mm and L_s = 500mm for the minor and major axes bending, respectively) were carefully designed so that the section moment capacity could be attained without the occurrence of shear failure. In three-point bending configuration, the total span of beam specimen was taken as twice of the shear span (L_s) of beam specimen subjected to four-point bending counterpart. The total specimen length (L) of each beam specimen is listed in Table 1.

2.2. Test setup and procedure

Two testing configurations of four-point bending and three-point bending were employed. The four-point bending tests were conducted to obtain the moment capacities and the moment-curvature relationships of specimens under constant moment. The setup of four-point bending tests is shown in Fig. 3. The pin-ended boundary conditions were simulated by a half-round support and roller supports. The specimens were seated on the customized made steel sittings. The steel sittings at the supports and the loading points together with the wooden blocks inserted inside the specimens at the loading locations were installed to prevent any possible local bearing failure and web crippling during testing. Three linear variable displacement transducers (LVDTs) were placed along the centerline of the tension face of each specimen at the two loading points and at the mid-span of the specimen to record the vertical deflections of the specimen. Hence, the curvature of each specimen could be obtained. The load was applied through a lockable special ball bearing and a spreader beam using displacement controlled loading method with a constant rate of 1.0 mm/min for all beam tests. The applied displacement was paused for 100 seconds near the ultimate load in order to obtain the static load. Therefore, static moment capacities were obtained. The applied load and the readings of the LVDTs were recorded at one second intervals during the tests.

The purpose of three-point bending tests was to obtain the moment capacities and the

moment-rotation relationships of specimens under a moment gradient. The setup of three-point bending tests is shown in Fig. 4. Similar to four-point bending, the pin-ended boundary conditions were simulated by a half-round support and roller supports. Two LVDTs were installed at each end of specimen to measure the end rotation whilst one LVDT was placed at the mid-span to measure the vertical displacement of the specimen. The three-point bending tests used the same test rig, loading method and data acquisition as the four-point bending tests.

2.3. Test results

For four point-bending tests, the static moment-curvature curves for specimens subjected to bending about the major and minor axes are plotted in Fig. 5. For three point-bending tests, the static moment-rotation curves for specimens subjected to bending about the major and minor axes are plotted in Fig. 6. No out-of-plane bending was observed in the tests. From the experimental results, it is observed that beams with stockier sections failed by material yielding (Y), whilst beams with less stocky sections failed by interaction of inelastic local buckling and material yielding (L+Y). The experimental moment capacities ($M_{Exp,4}$ and $M_{Exp,3}$) and failure modes of EHS beam specimens under constant moment and a moment gradient are summarized in Table 3. It is found that the results of repeated tests are very close to their corresponding first test values. The small differences between the repeated test values and their corresponding first test values demonstrated the reliability of the test results. In this study, it can be observed from the test results of EHS under constant moment that EHS with larger cross-section aspect ratio generally exhibited more ductile behavior than that with smaller aspect ratio. It is worth noting that for the same cross-section, specimen under a moment gradient reached a higher moment capacity than its counterpart that was subjected to constant moment by 13% on average.

3. Numerical modeling

3.1. Finite element models

In parallel with the experimental investigation, finite element (FE) models were established by using the FE analysis package ABAQUS of version 6.14 to simulate the beam tests and to

perform parametric study. The measured cross-section geometries as reported in Table 1, the measured Young's modulus and the converted true plastic stress-strain responses were used. Full length of beam specimens was modeled.

To replicate the four-point and three-point bending test configurations, the roller supports and half-round support with the customized made steel sittings and the wooden blocks were simulated by coupling the displacements of the half cross-section in the loading/supporting regions to the displacements of the corresponding reference points located at the cross-section centerline and 75 mm away from the tip of contacting points of specimens at the middle of loading/supporting regions. The in-plane displacements of the reference points related to the roller supports were unrestrained, while all out-of-plane displacements of the reference points and the translation of the reference point corresponding to the half-round support were restrained.

Shell element with four nodes and reduced integration (S4R) was selected as commonly adopted in the FE models of steel members [25-34]. The minimum of 20 mm and $B/20+(D-B)/10\pi$ was taken as the mesh size of the models. The mesh was assigned uniformly in the circumferential and longitudinal directions to the EHS beam models.

The longitudinal residual stresses induced during the forming process have more dominant effect upon the structural performance of steel members than the residual stresses in transverse direction. In longitudinal direction, the magnitude of bending residual stress is much larger than that of membrane residual stress for cold-formed steel EHS investigated in this study as reported by Chen and Young [17]. Therefore, it is rational not to explicitly incorporate the residual stresses in the beam models since the bending residual stress with larger magnitude and more significant effect has been inherently incorporated into the measured material properties obtained from coupon tests, whilst the membrane residual stress has negligibly small influence on the results of modeling tests [27, 29, 35, 36].

In general, the material strength in the curviest portion of cold-formed steel EHS was enhanced during the cold-forming process as compared to the strength in the flattest portion. The cold-forming effect on material strength enhancement of EHS should be considered in the FE models by adopting the methodology proposed by Chen and Young [17]. The strength enhancement at the curviest portion of EHS was extended from the tips of the section to a certain distance as expressed by the fractions of the larger dimension of the median-profile of EHS (D_m/3, D_m/4, D_m/6 and D_m/10) as shown in Fig. 7. Sensitivity analysis was conducted, and the results as shown in Table 4 indicate that different fractions of D_m provide similar flexural strength predictions with the average difference of 5%. Therefore, it is rational to adopt the fraction value of D_m/6 in the model validation and parametric study, as consistently used in the cold-formed steel EHS stub column model [17] and pin-ended column model [16].

The initial local geometric imperfection pattern was taken as the lowest elastic local buckling mode shape in eigenvalue analysis. The buckling mode shape was further amplified by a certain magnitude of imperfection. The sensitivity study was also performed to determine the suitable magnitude of local imperfection to be adopted in the model validation and parametric study. The results show that different magnitudes of local imperfection provide similar FE strength predictions with the average difference of 4%. The magnitude of t/50 was selected for local imperfection in the beam models, which was consistently adopted in the cold-formed steel EHS stub column model [17] and pin-ended column model [16].

3.2. Validation of finite element models

Based on the aforementioned modeling parameters and assumptions, the finite element models were developed and validated against 20 beam tests. The second last column of Table 4 shows the validation results. The finite element models can successfully replicate the flexural capacities of the beam specimens as evident by the mean value and coefficient of variation (COV) of the test-to-FE strength ratio of 0.96 and 0.087, respectively. The comparisons of moment-curvature and moment-rotation responses obtained from the tests and finite element

models for typical test specimens are presented in Figs. 8 and 9, respectively. The failure modes can also be captured by the finite element analysis as shown in Figs. 10 and 11.

3.3. Parametric study

The validated FE model for four-point bending test was used to perform extensive parametric study on cold-formed steel EHS under constant moment. Material properties at the flattest and curviest portions of EHS 140×85×3 were used. Finite element analyses on a total of 235 beam specimens were conducted, which comprised 104 and 141 beams in the major and minor axes bending, respectively. A wide range of cross-section dimensions was covered in the parametric study. The cross-section aspect ratio of the EHS varied from 1.25 to 3.50. The larger dimension of the section (D) varied from 150 to 500 mm. Since the expression of cross-section slenderness is not well defined in the current international design specifications [18-20, 37, 38], the equivalent diameter (D_e) defined by Chan *et al.* [14] was adopted to examine the coverage of cross-section slenderness in this study. The cross-section slenderness (D_e/t) ranged from 11 to 211 and 16 to 528 for beams bent about the major and minor axes, respectively. The shear span was carefully designed to avoid the occurrence of shear failure, and the moment span was taken as the maximum of 3 times the larger dimension of EHS and the length of designed shear span. Table 5 summarizes the details of beam specimens and the corresponding flexural strengths obtained from the numerical study. The ultimate moment to plastic moment ratio (M_u/M_{pl}) for EHS with five typical cross-section aspect ratios in two different bending directions is plotted against the cross-section slenderness (D_e/t) in Fig. 12 to show the effects of different parameters on the moment capacity of EHS beam members. From Fig. 12, the moment capacity of EHS as represented by the moment ratio (M_u/M_{pl}) decreases with the increase of cross-section slenderness as expected. For EHS with the same cross-section slenderness, EHS beams with larger cross-section aspect ratio possess higher moment capacity than the counterparts with smaller cross-section aspect ratio, and EHS beams in major axis bending generally possess higher moment capacity than the counterparts in minor axis bending. For EHS subjected to major axis bending, the corresponding value of cross-section slenderness when the moment ratio equals to unity increases with the cross-section aspect ratio. Whilst for EHS subjected

to minor axis bending, the corresponding values of cross-section slenderness when the moment ratio equals to unity are similar for different cross-section aspect ratios.

4. Reliability analysis

The test and finite element strengths were compared with the design strengths predicted by the equivalent diameter method [14], equivalent RHS approach [15], various international design specifications [18-20] by adopting equivalent diameter as well as the Direct Strength Method [18] and the Continuous Strength Method [21-23]. The reliability of these design methods for nominal strength (unfactored design strength) predictions of cold-formed steel EHS beam members was evaluated by reliability analysis as detailed in the North American Specification AISI-S100 [18]. The lower bound limit of reliability index (β) is taken to be 2.5, below which the design method is considered to be unreliable. The values of statistical parameters included in the calculation of reliability index are specified in the AISI-S100 [18]. The load combination of 1.35DL+1.5LL was used for the equivalent diameter method, equivalent RHS approach and the Continuous Strength Method, whilst 1.2DL+1.6LL was used for the North American (including the DSM) and American Specifications, where DL and LL mean the dead load and live load, respectively. For Australian Standard, the load combination of 1.2DL+1.5LL was adopted in the reliability analysis. Different values of resistance factor (ϕ) were used for different design methods as shown in Table 6.

5. Assessment of existing design methods

5.1. General

The current design rules for structural steel design [18-20, 37, 38] do not cover the flexural design of cold-formed steel elliptical hollow sections. The moment capacities of cold-formed steel EHS beams obtained from the tests and parametric study were compared with the design strengths predicted by the equivalent diameter method [14], equivalent RHS approach [15], the traditional design methods [18-20] using equivalent diameter as well as the DSM [18] and the CSM [21-24]. The material properties at the location with the lowest 0.2% proof stress were used in nominal

strength calculation for conservative predictions.

5.2. Equivalent diameter method proposed by Chan *et al.* [14]

On the basis of the results obtained from the investigation on hot-finished steel EHS, the equivalent diameter method was proposed for the cross-section classification and design strength predictions of hot-finished steel elliptical hollow sections [14]. For EHS beams, the equivalent diameters of EHS subjected to the major and minor axes bending can be expressed by Eqs. (1) and (2), respectively. A new set of Class 1, Class 2 and Class 3 slenderness limit ($D_e/t\varepsilon^2$) of 50, 70, 140 was proposed for EHS in flexure, respectively. If the slenderness limit reaches beyond 140, the EHS is classified as slender section and the effective section modulus (W_{eff}) is calculated as per Eq. (3). Subsequently, the design flexural strength of EHS (M_{Chan}) can be predicted by Eq. (4) proposed by Chan *et al.* [14]. The applicability of the equivalent diameter method for the design of cold-formed steel elliptical hollow section beam members was assessed herein.

$$\text{Major axis bending:} \quad D_e = \begin{cases} 0.4\frac{D^2}{B} & \text{for } \frac{D}{B} > 1.357 \\ \frac{B^2}{D} & \text{for } \frac{D}{B} \leq 1.357 \end{cases} \tag{1}$$

$$\text{Minor axis bending:} \quad D_e = \frac{D^2}{B} \tag{2}$$

$$W_{eff} = W_{el}\left[\frac{140}{D_e/(t\varepsilon^2)}\right]^{0.25} = W_{el}\left[\frac{140}{D_e/t}\frac{235}{f_y}\right]^{0.25} \tag{3}$$

$$M_{Chan} = \begin{cases} W_{pl}f_y & \text{for } \frac{D_e}{t\varepsilon^2} \leq 70 \\ W_{el}f_y & \text{for } 70 < \frac{D_e}{t\varepsilon^2} \leq 140 \\ W_{eff}f_y & \text{for } \frac{D_e}{t\varepsilon^2} > 140 \end{cases} \tag{4}$$

where f_y is the yield stress, W_{el} and W_{pl} are the elastic and plastic section moduli, respectively.

The flexural strengths of EHS beam specimens obtained from the tests and parametric study were compared with the nominal flexural strengths (unfactored design flexural strengths) predicted by the equivalent diameter method proposed by Chan *et al.* [14] as shown in Table 6 and Fig. 13. The equivalent diameter method provides quite conservative and scattered design strength predictions for cold-formed steel EHS beams as evident by the mean value and corresponding COV

of M_u/M_{Chan} being 1.28 and 0.130, respectively. The corresponding reliability index is 2.67 with the resistance factor of 1.0. These indicate that the design flexural strength predictions by the equivalent diameter method [14] is reliable though the predictions are quite conservative and scattered.

5.3. Equivalent RHS approach proposed by Haque *et al.* [15]

As reported by Haque *et al.* [15], the local buckling of EHS resembles plate buckling more than shell buckling. Equivalent RHS approach was therefore proposed for cross-section classification and design strength predictions based on the investigation results of hot-finished steel EHS. Different equivalent RHS shapes have been proposed by Haque *et al.* [15] for EHS subjected to bending about the major and minor axes as expressed by Eqs. (5) and (6), respectively.

$$\text{Major axis bending:} \quad B_e = \frac{A-2Dt+4t^2}{2t}; \; H_e = D \tag{5}$$

$$\text{Minor axis bending:} \quad H_e = \frac{A-2Bt+4t^2}{2t}; \; B_e = B \tag{6}$$

where A is the cross-section area of EHS, B_e and H_e are the width and height of the equivalent RHS, respectively.

With the geometries of equivalent RHS, each element can be classified based on the new set of slenderness limits proposed by Haque *et al.* [15], the equivalent section modulus and hence the design flexural strength can be calculated. Since the equivalent RHS approach was proposed based on the results of hot-finished steel EHS, assessment on its applicability for the design of cold-formed steel EHS beams is required.

The flexural capacities of beam specimens obtained from the tests and parametric study were compared with the design flexural strengths predicted by the equivalent RHS approach proposed by Haque *et al.* [15] as shown in Table 6 and Fig. 14. The mean value of M_u/M_{Haque} is 1.11 with the corresponding COV of 0.210. The equivalent RHS approach provides less conservative but more scattered predictions compared to the equivalent diameter method. The reliability index is 1.84 with

the resistance factor of 1.0, indicating that the equivalent RHS approach [15] is not reliable in predicting the design strengths of cold-formed steel EHS beam members.

5.4. Existing traditional design rules using equivalent diameter

The current traditional design rules for tubular steel structures [18-20, 37, 38] cover the cross-section classification and flexural design for circular hollow sections (CHS) with constant curvature around the cross-section profile, but not for EHS with continuous change of curvature around the section profile. By adopting the equivalent diameters proposed by Chan *et al.* [14] for EHS subjected to the major and minor axes bending, the design rules originally developed for CHS as detailed in the Australian Standard [20], the North American [18] and American Specifications [19] were used to predict the design strengths of cold-formed steel EHS beam members. The upper limits of cross-section slenderness (D_e/t) specified in various design rules were released to assess the suitability of existing design rules with the equivalent diameter adopted for the design strength predictions of cold-formed steel EHS beams.

The flexural strengths of EHS beams obtained from experimental and numerical investigation in this study were compared with the design flexural strengths predicted by the Australian Standard [20], the North American [18] and American Specifications [19] with the equivalent diameter adopted as shown in Table 6 and from Figs. 15 to 17. The mean values of $M_u/M_{AS4100}^{\dagger}$, $M_u/M_{AISI}^{\dagger}$ and $M_u/M_{AISC}^{\dagger}$ are 1.49, 1.23 and 1.18 with the corresponding COV of 0.547, 0.130 and 0.143 for design strengths predicted by the Australian Standard [20], the North American [18] and American Specifications [19], respectively. The resulted reliability indices are 1.61, 2.84 and 2.81 with the resistance factors of 0.90, 0.95 and 0.90 for the Australian Standard [20], the North American [18] and American Specifications [19], respectively. By using the equivalent diameters proposed by Chan *et al.* [14], the North American [18] and American Specifications [19] provide quite conservative and scattered design strength predictions for cold-formed steel EHS beam members in a reliable manner, whilst the Australian Standard [20] is not capable in predicting the design strengths of cold-formed steel EHS beams.

5.5. Direct Strength Method

The Direct Strength Method as detailed in Chapter F of the AISI-S100 [18] does not require the cross-section classification prior to the design strength predictions. The nominal flexural strength is determined by the minimum of the nominal flexural strengths for lateral-torsional buckling, local buckling and distortional buckling. Only local buckling was considered herein since no lateral-torsional buckling or distortional buckling was observed for EHS in this study.

In the calculation of nominal flexural strength for local buckling, the critical elastic local buckling moment of EHS was obtained from CUFSM program [39] using the finite strip method. Followed by critical elastic local buckling moment determination, the moment capacity (M_{DSM}) was calculated accordingly. The flexural capacities of beam specimens obtained from the tests and parametric study were compared with the design flexural strengths predicted by the DSM without consideration of inelastic reserve capacity as shown in Table 6, Figs. 18 and 19. The mean value of M_u/M_{DSM} is 1.34 with the corresponding COV of 0.132. It is found that the Direct Strength Method provides quite conservative and scattered predictions for cold-formed steel EHS beam members in this study.

For the approach with consideration of inelastic reserve capacity in the Direct Strength Method, the moment capacity ($M_{DSM,IR}$) was calculated according to Clause F3.2.3 of the AISI-S100 [18]. The flexural capacities of specimens obtained from the tests and parametric study were compared with the design flexural strengths predicted by the DSM with consideration of inelastic reserve capacity as shown in Table 6 and Fig. 20. It is shown that the mean value of $M_u/M_{DSM,IR}$ is 1.10 with the corresponding COV of 0.074, which is less conservative and less scattered than the calculation without consideration of inelastic reserve capacity.

The resulted reliability indices are 2.85 and 3.34 with the resistance factor of 0.90 for the design strength predictions by the DSM with and without consideration of inelastic reserve capacity, respectively, indicating that both approaches provide conservative and reliable design strength

predictions for cold-formed steel EHS under bending. However, further improvement remains possible.

5.6. Continuous Strength Method

The deformation-based design approach, Continuous Strength Method, was developed recently and codified in the AISC Design Guide 30 for design of structural stainless steel [23]. The material model for cold-formed structural steel sections proposed by Buchanan *et al.* [21] was adopted herein for cold-formed steel EHS to account for the strain hardening of material. The base curves for RHS (including square hollow section) and CHS were used in the RHS and CHS approaches of the CSM to assess the applicability of these two approaches for the design flexural strength predictions of cold-formed steel EHS beams.

The results obtained from experimental and numerical investigation in this study were compared with the design strength predictions by the RHS and CHS approaches of the CSM as shown in Table 6, Figs. 21 and 22. The mean values of $M_u/M_{CSM,RHS}$ and $M_u/M_{CSM,CHS}$ are 0.98 and 1.16 with the corresponding COV values of 0.070 and 0.121 for the RHS and CHS approaches of the CSM, respectively. The reliability indices are 1.82 and 2.34 for the RHS and CHS approaches of the CSM, respectively, with the resistance factor of 1.0. The results show that the RHS approach of the CSM provides slightly unconservative predictions, especially for beams subjected to the minor axis bending, whilst the CHS approach provides quite conservative and scattered predictions for cold-formed steel EHS beam members. In addition, both approaches of the CSM are not reliable. Therefore, modification on the Continuous Strength Method for cold-formed steel EHS beams can be proposed.

6. Modified design methods

6.1. Modified Direct Strength Method

The applicability of existing DSM with and without consideration of inelastic reserve capacity for the design strength predictions of cold-formed steel EHS beams was examined in

previous section. The predictions are quite conservative and scattered, especially for compact EHS as shown in Fig. 18. Due to the curved cross-section profile of EHS, most parts of EHS were subjected to low stress level when the extreme fiber reaches the yield stress due to the existence of strain gradient along the depth of the cross-section. Therefore, it is very likely that the moment capacity of EHS beam, especially for beam with compact section, reaches beyond the yield moment (M_y). The DSM design equation was modified as expressed by Eq. (7). The nominal flexural strength predicted by the modified DSM (M_{DSM}*) was equal to M_{nl}* with consideration of local buckling only since no distortional or lateral-torsional buckling was observed.

$$M_{nl}{}^{*} = \begin{cases} \left(1.6 - 1.06\sqrt{\frac{M_y}{M_{crl}}}\right) M_y & \text{for } \lambda_l \leq 0.566 \\ 0.6\left(\frac{M_{crl}}{M_y}\right)^{0.45} M_y & \text{for } \lambda_l > 0.566 \end{cases} \tag{7}$$

The flexural strengths obtained from the tests and FE analyses were compared with the design strengths predicted by the modified DSM as shown in Table 6, Figs. 18 and 23. The mean value and the corresponding COV of M_u/M_{DSM}* is 1.05 and 0.069, respectively. The accuracy of design strength predictions of cold-formed steel EHS beams is improved by adopting the modified DSM. The resulted reliability index is 2.68 with the proposed resistance factor of 0.9, indicating that the modified DSM is reliable.

6.2. Modified Continuous Strength Method

Modified base curve for EHS has been proposed by Chen and Young [17] as shown in Eq. (8). The applicability of the modified CSM with the modified base curve incorporated for the design flexural strength predictions of cold-formed steel EHS beams was assessed.

$$\left(\frac{\varepsilon_{csm}}{\varepsilon_y}\right)_{EHS} = \begin{cases} \frac{0.308}{\lambda_{CSM}{}^{1.8}} \leq \text{lesser}\left(15, \frac{0.4\varepsilon_u}{\varepsilon_y}\right) & \text{for } \lambda_{CSM} \leq 0.52 \\ \left(1 - \frac{0.219}{\lambda_{CSM}{}^{0.6}}\right) \frac{1}{\lambda_{CSM}{}^{0.6}} & \text{for } \lambda_{CSM} > 0.52 \end{cases} \tag{8}$$

The experimental and numerical results obtained from this study were compared with the design predictions by the modified CSM as shown in Table 6 and Fig. 24. The mean M_u/M_{CSM}* is

1.04 and the corresponding COV is 0.049. The modified CSM provides generally conservative and less scattered design predictions for beams subjected to bending about the major and minor axes. The reliability index is 2.54 with the proposed resistance factor of 0.9 as consistently adopted in the modified DSM. The results indicate that the modified CSM is capable to provide accurate and the least scattered design strength predictions among all design methods for cold-formed steel EHS beams in a reliable manner.

7. Conclusions

Experimental and numerical studies on the structural behavior of cold-formed steel elliptical hollow section beams are presented in this paper. Twenty beam tests were conducted on cold-formed steel elliptical hollow sections bent about the major and minor axes in both four-point and three-point bending configurations. Following the test program, an extensive numerical study was carried out on beam specimens with a wide range of cross-section geometries. The 245 experimental and numerical data were used to evaluate the applicability and reliability of the equivalent diameter method, equivalent RHS approach, the traditional design rules using equivalent diameter as well as the Direct Strength Method and the Continuous Strength Method. The results show that these design methods are not able to provide accurate design strength predictions for cold-formed steel elliptical hollow section beam members in a reliable manner. Therefore, modifications on the Direct Strength Method and the Continuous Strength Method as well as a resistant factor of 0.9 are proposed in this study. The modified Direct Strength Method provides reliable predictions with improved accuracy, and the modified Continuous Strength Method provides generally conservative, the least scattered and reliable design strength predictions. It is recommended to use either of the modified design methods for the flexural strength predictions of cold-formed steel elliptical hollow section beams.

Acknowledgements

The authors are grateful to Shenyang Dongyang Special Section Tube for supplying the test specimens. The authors are also thankful to Miss Hoi-Kiu CHAN for her assistance in the experimental program as part of her final year undergraduate research project at The University of Hong Kong. The research work described in this paper was supported by a grant from the Research Grants Council of the Hong Kong Special Administrative Region, China (Project No. 17267416).

Nomenclature

A	Area of the section
B	The smaller outer diameter of the section
B_e	Width of the equivalent RHS
COV	Coefficient of variation
CSM	Continuous strength method
D	The larger outer diameter of the section
D_e	Equivalent diameter of elliptical hollow section
D_m	The larger dimension of the median-profile of the section
DSM	Direct strength method
E	Young's modulus
EHS	Elliptical hollow section
f_y	Yield stress
H_e	Height of the equivalent RHS
L	Total specimen length
L_m	Moment span
L_s	Shear span
$M_{AISC}^{\dagger}$	Nominal flexural strength predicted by American Specification ANSI/AISC360 [19] with equivalent diameter
$M_{AISI}^{\dagger}$	Nominal flexural strength predicted by North American Specification AISI-S100 [18] with equivalent diameter

$M_{AS4100}^{\dagger}$ Nominal flexural strength predicted by Australian Standard AS4100 [20] with equivalent diameter

M_{Chan} Nominal flexural strength of beam predicted by the equivalent diameter method proposed by Chan *et al.* [14]

M_{crl} Critical elastic local buckling moment of beam

$M_{CSM,CHS}$ Nominal flexural strength of beam predicted by the CHS approach in the Continuous Strength Method

$M_{CSM,RHS}$ Nominal flexural strength of beam predicted by the RHS approach in the Continuous Strength Method

M_{CSM}* Nominal flexural strength of beam predicted by the modified Continuous Strength Method

M_{DSM} Nominal flexural strength of beam predicted by the Direct Strength Method without consideration of inelastic reserve capacity

$M_{DSM,IR}$ Nominal flexural strength of beam predicted by the Direct Strength Method with consideration of inelastic reserve capacity

M_{DSM}* Nominal flexural strength of beam predicted by the modified Direct Strength Method

M_{Exp} Experimental moment capacity

$M_{Exp,3}$ Moment capacity for section in three-point bending

$M_{Exp,4}$ Moment capacity for section in four-point bending

M_{FE} Finite element moment capacity

M_{Haque} Nominal flexural strength of beam predicted by the equivalent RHS approach proposed by Haque *et al.* [15]

M_{nl}* Nominal flexural strength of beam for local buckling

M_{pl} Plastic moment of cross-section

M_u Ultimate moment capacity

M_y Yield moment of beam

n Ramberg-Osgood parameter

t Thickness of the section

TC	Tensile coupon specimen
W_{eff}	Effective section modulus
W_{el}	Elastic section modulus
W_{pl}	Plastic section modulus
β	Reliability index
ε_{csm}	Limiting strain for the cross-section
ε_f	Tensile strain at fracture
ε_u	Ultimate strain
ε_y	Yield strain
ϕ	Resistance factor
λ_l	Slender factor for local buckling
λ_{CSM}	Cross-section slenderness in the Continuous Strength Method
σ_u	Static ultimate tensile strength of material
$\sigma_{0.2}$	Static 0.2% tensile proof stress of material

References

[1] Lai MH, Ho JCM. Confinement effect of ring-confined concrete-filled-steel-tube columns under uni-axial load. Engineering Structures 2014;67:123-141.

[2] Lai MH, Ho JCM. A theoretical axial stress-strain model for circular concrete-filled-steel-tube columns. Engineering Structures 2016;125:124-143.

[3] Chan TM, Gardner L. Bending strength of hot-rolled elliptical hollow sections. Journal of Constructional Steel Research 2008;64(9):971-986.

[4] Chan TM, Gardner L. Compressive resistance of hot-rolled elliptical hollow sections. Engineering Structures 2008;30(2):522-532.

[5] Chan TM, Gardner L. Flexural buckling of elliptical hollow section columns. Journal of structural engineering 2009;135(5):546-557.

[6] Gardner L, Chan TM. Cross-section classification of elliptical hollow sections. Steel and Composite Structures 2007;7(3):185-200.

[7] Gardner L, Chan TM, Wadee MA. Shear response of elliptical hollow sections. Structures and Buildings 2008;161(6):301-309.

[8] Insausti A, Gardner L. Analytical modelling of plastic collapse in compressed elliptical hollow sections. Journal of Constructional Steel Research 2011;67(4):678-689.

[9] Law KH, Gardner L. Lateral instability of elliptical hollow section beams. Engineering Structures 2012;37:152-166.

[10] Law KH, Gardner L. Buckling of elliptical hollow section members under combined compression and uniaxial bending. Journal of Constructional Steel Research 2013;86:1-16.

[11] Silvestre N, Gardner L. Elastic local post-buckling of elliptical tubes. Journal of Constructional Steel Research 2011;67(3):281-292.

[12] Theofanous M, Chan TM, Gardner L. Structural response of stainless steel oval hollow section compression members. Engineering Structures 2009;31(4):922-934.

[13] Theofanous M, Chan TM, Gardner L. Flexural behaviour of stainless steel oval hollow sections. Thin-Walled Structures 2009;47(6):776-787.

[14] Chan TM, Gardner L, Law KH. Structural design of elliptical hollow sections: a review. Proceedings of the Institution of Civil Engineers-Structures and Buildings 2010;163(6):391-402.

[15] Haque T, Packer JA, Zhao XL. Equivalent RHS approach for the design of EHS in axial compression or bending. Advances in Structural Engineering 2012;15(1):107-120.

[16] Chen MT, Young B. Structural performance of cold-formed steel elliptical hollow section pin-ended columns. Thin-Walled Structures 2018 (In press) https://doi.org/10.1016/j.tws.2018.11.024.

[17] Chen MT, Young B. Material properties and structural behavior of cold-formed steel elliptical hollow section stub columns. Thin-Walled Structures 2019;134:111-126.

[18] AISI-S100 2016. North American Specification for the design of cold-formed steel structural members. *AISI S100-16.* Washington,D.C., USA: American Iron and Steel Institute.

[19] ANSI/AISC360 2016. Specification for Structural Steel Buildings. *ANSI/AISC 360-16.* Chicago, IL, USA: American Institute of Steel Construction.

[20] AS4100 1998. Steel structures. *AS 4100: 1998.* Homebush, New South Wales, Australia: Standards Australia.

[21] Buchanan C, Gardner L, Liew A. The continuous strength method for the design of circular hollow sections. Journal of Constructional Steel Research 2016;118:207-216.

[22] Gardner L. The continuous strength method. Structures and Buildings 2008;161(3):127-133.

[23] AISC 2013. Structural Stainless Steel. *AISC Design Guide 30.* American Institute of Steel Construction.

[24] Yun X, Gardner L. The continuous strength method for the design of cold-formed steel non-slender tubular cross-sections. Engineering Structures 2018;175:549-564.

[25] Chen MT, Young B. Cross-sectional behavior of cold-formed steel semi-oval hollow sections. Engineering Structures 2018;177:318-330.

[26] Chen MT, Young B. Experimental and numerical investigation on pin-ended cold-formed steel semi-oval hollow section compression members. Journal of Constructional Steel Research 2018;151:174-184.

[27] Huang Y, Young B. Experimental and numerical investigation of cold-formed lean duplex stainless steel flexural members. Thin-Walled Structures 2013;73:216-228.

[28] Ma JL, Chan TM, Young B. Design of cold-formed high strength steel tubular beams. Engineering Structures 2017;151:432-443.

[29] Zhao O, Rossi B, Gardner L, Young B. Behaviour of structural stainless steel cross-sections under combined loading–Part II: Numerical modelling and design approach. Engineering Structures 2015;89:247-259.

[30] Li HT, Young B. Tests of cold-formed high strength steel tubular sections undergoing web crippling. Engineering Structures 2017;141:571-583.

[31] Lan X, Chan T-M, Young B. Static strength of high strength steel CHS X-joints under axial compression. Journal of Constructional Steel Research 2017;138:369-379.

[32] Lan X, Chan T-M, Young B. Structural behaviour and design of chord plastification in high strength steel CHS X-joints. Construction and Building Materials 2018;191:1252-1267.

[33] Yun X, Gardner L. Numerical modelling and design of hot-rolled and cold-formed steel continuous beams with tubular cross-sections. Thin-Walled Structures 2018;132:574-584.

[34] Yun X, Gardner L, Boissonnade N. Ultimate capacity of I-sections under combined loading–Part 1: Experiments and FE model validation. Journal of Constructional Steel Research 2018;147:408-421.

[35] Huang Y, Young B. Structural performance of cold-formed lean duplex stainless steel columns. Thin-Walled Structures 2014;83:59-69.

[36] Ma JL, Chan TM, Young B. Experimental Investigation on Stub-Column Behavior of Cold-Formed High-Strength Steel Tubular Sections. Journal of Structural Engineering 2015;142(5):04015174.

[37] AS/NZS4600 2005. Cold-formed steel structure. *AS/NZS 4600:2005.* Sydney, Australia: Standards Australia/Standards New Zealand.

[38] EN1993-1-1 2005. Design of steel structures–Part 1.1: General rules and rules for buildings. *EN 1993-1-1:2005.* Brussels, Belgium: European Committee for Standardization.

[39] Schafer BW, Ádány S. Buckling analysis of cold-formed steel members using CUFSM: conventional and constrained finite strip methods. In: Eighteenth International Specialty Conference on Cold-Formed Steel Structures, Orlando, FL, USA; 2006. 39-54.

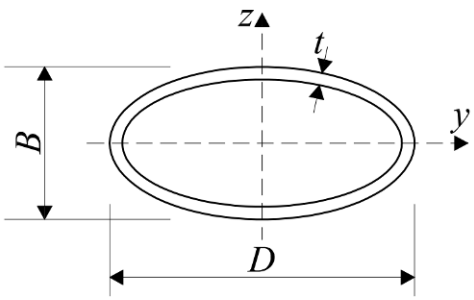

Fig. 1. Cross-section geometry of EHS

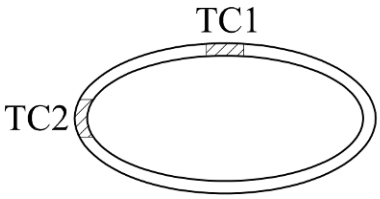

Fig. 2. Locations of tensile coupon specimens

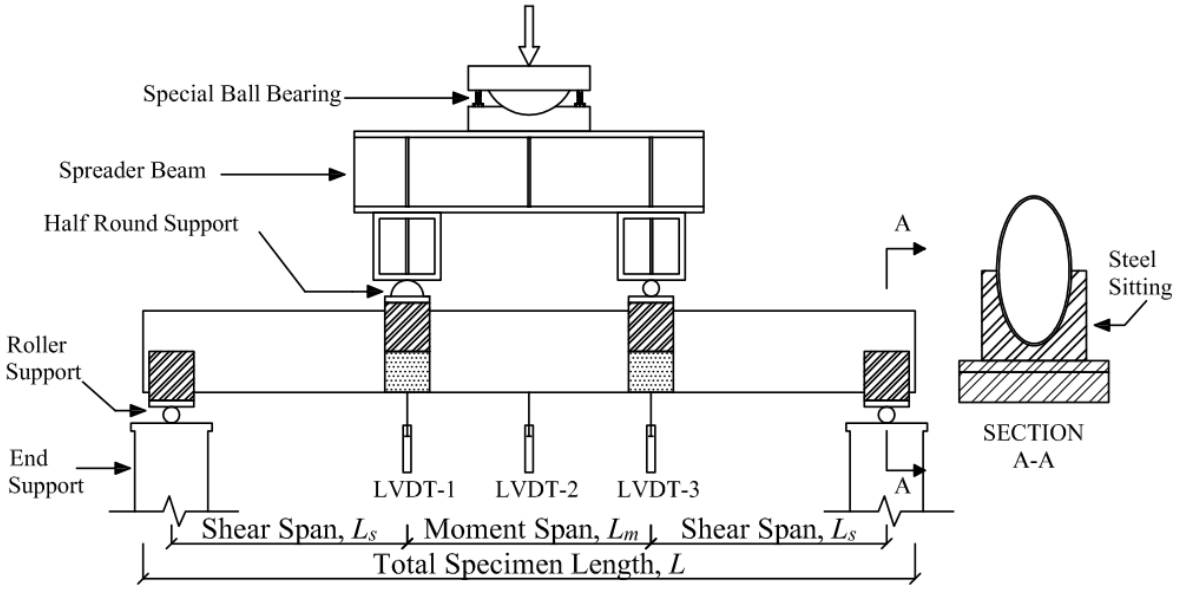

(a) Schematic setup of four-point bending test

(b) Experimental setup of four-point bending test

Fig. 3. Setup of EHS beam test in four-point bending configuration

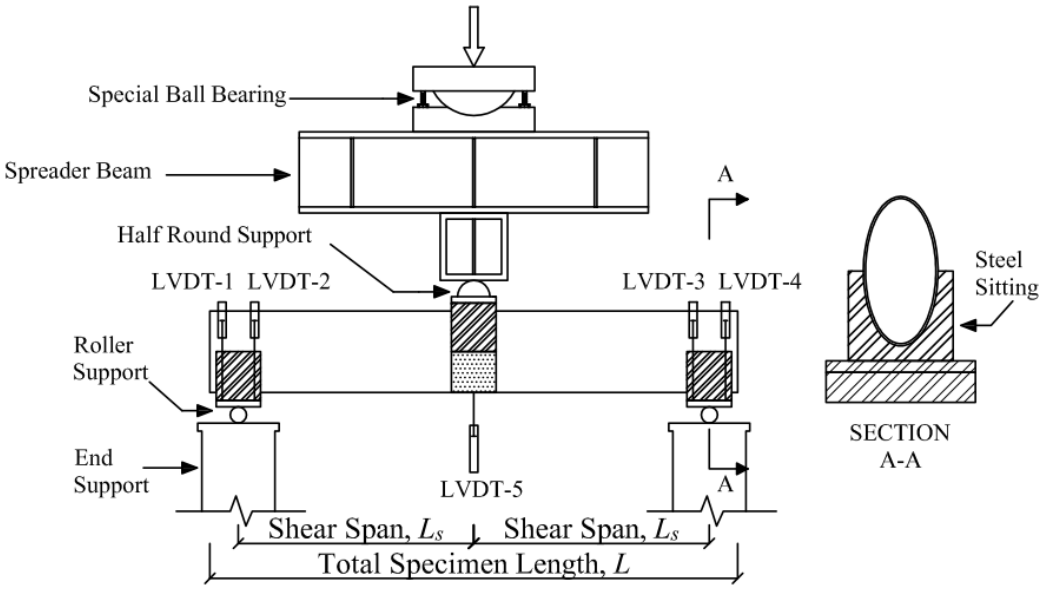

(a) Schematic setup of three-point bending test

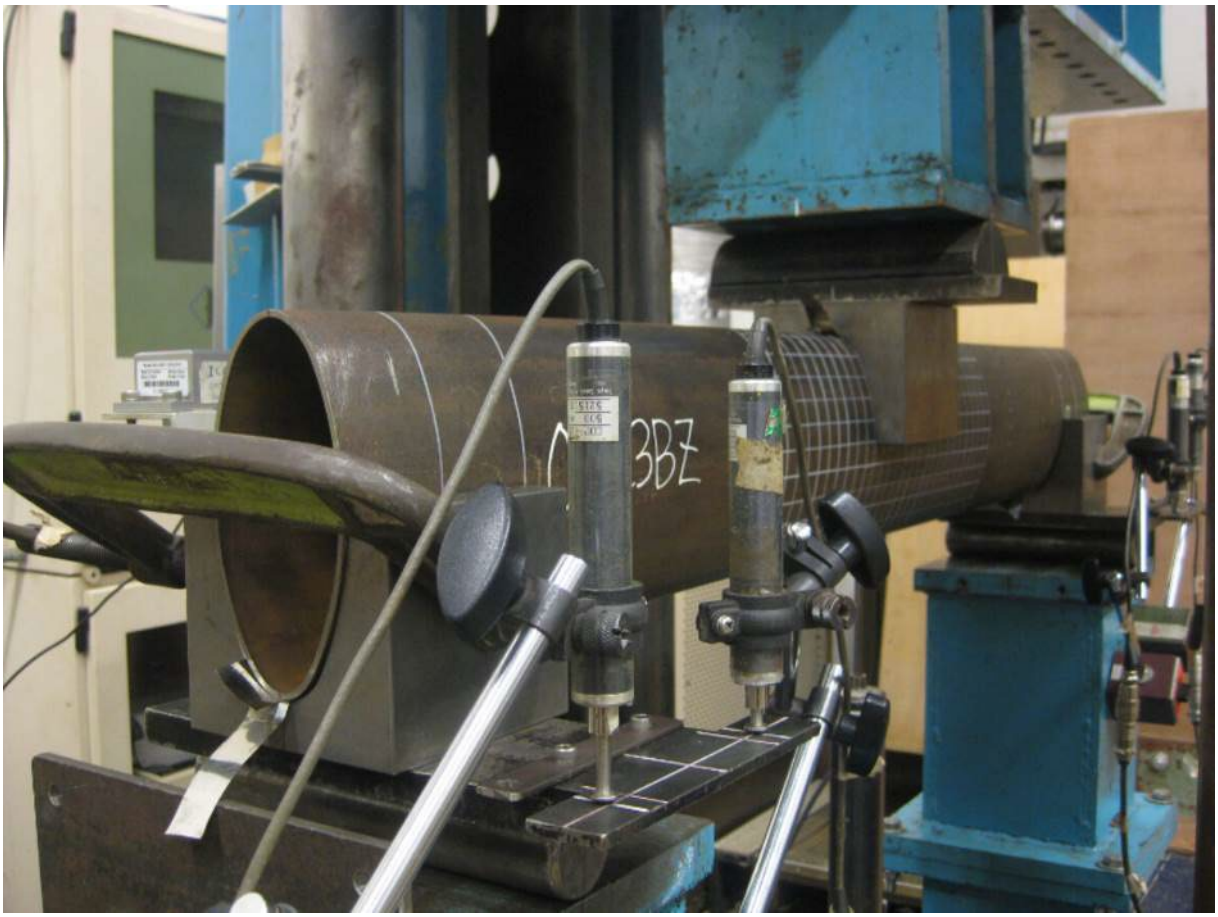

(b) Experimental setup of three-point bending test

Fig. 4. Setup of EHS beam test in three-point bending configuration

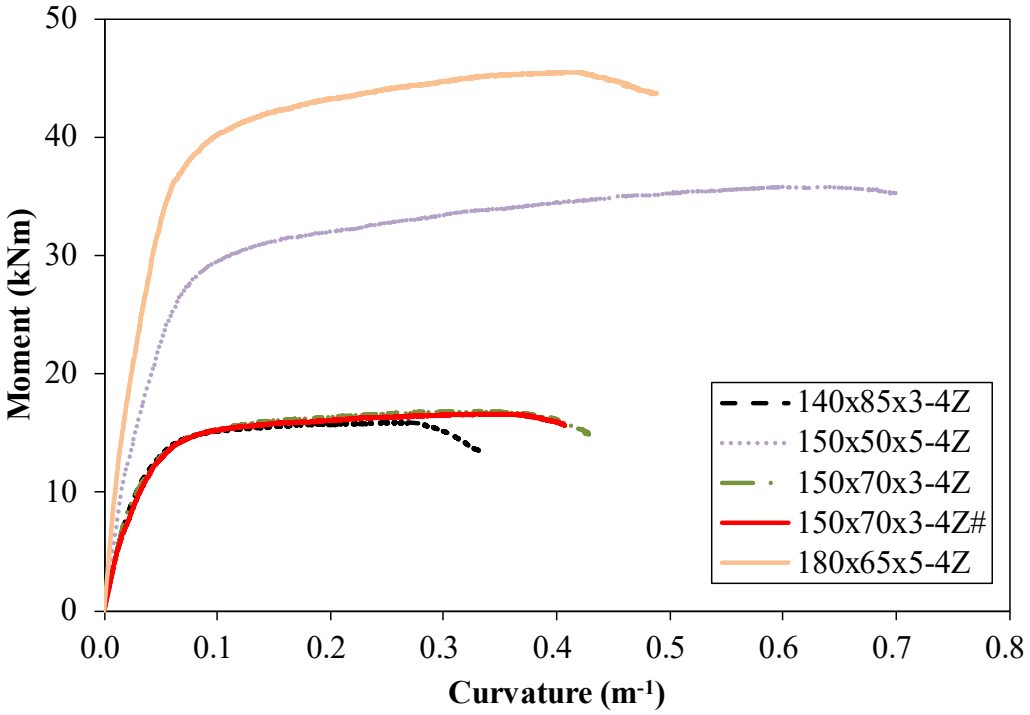

(a) Major axis bending

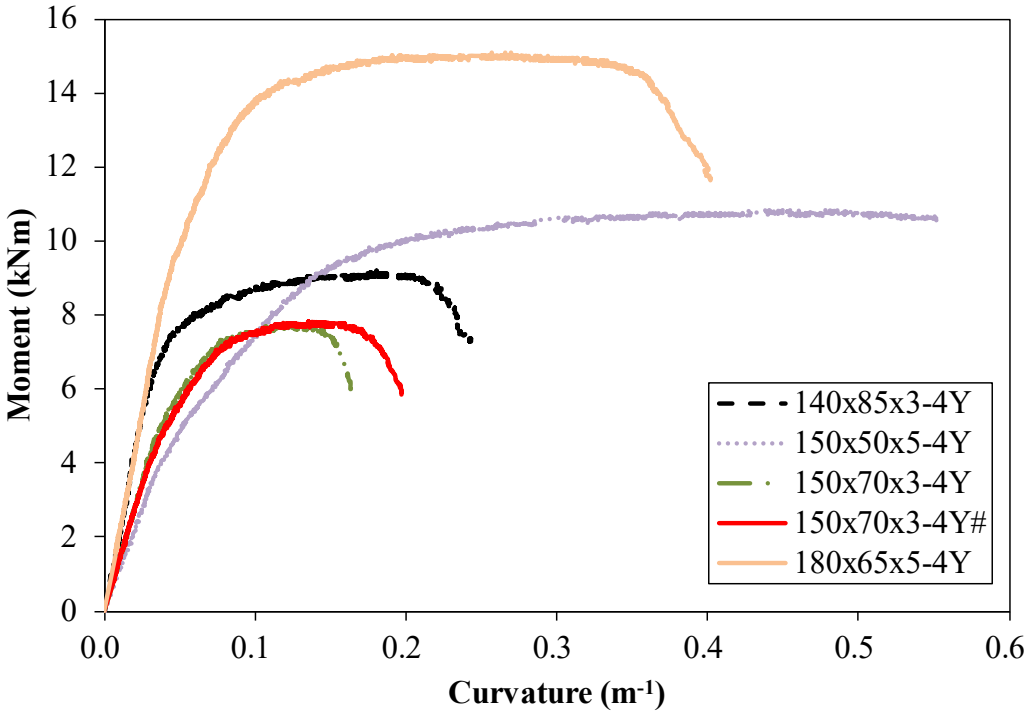

(b) Minor axis bending

Fig. 5. Moment-curvature relationship of EHS beam members subjected to four-point bending

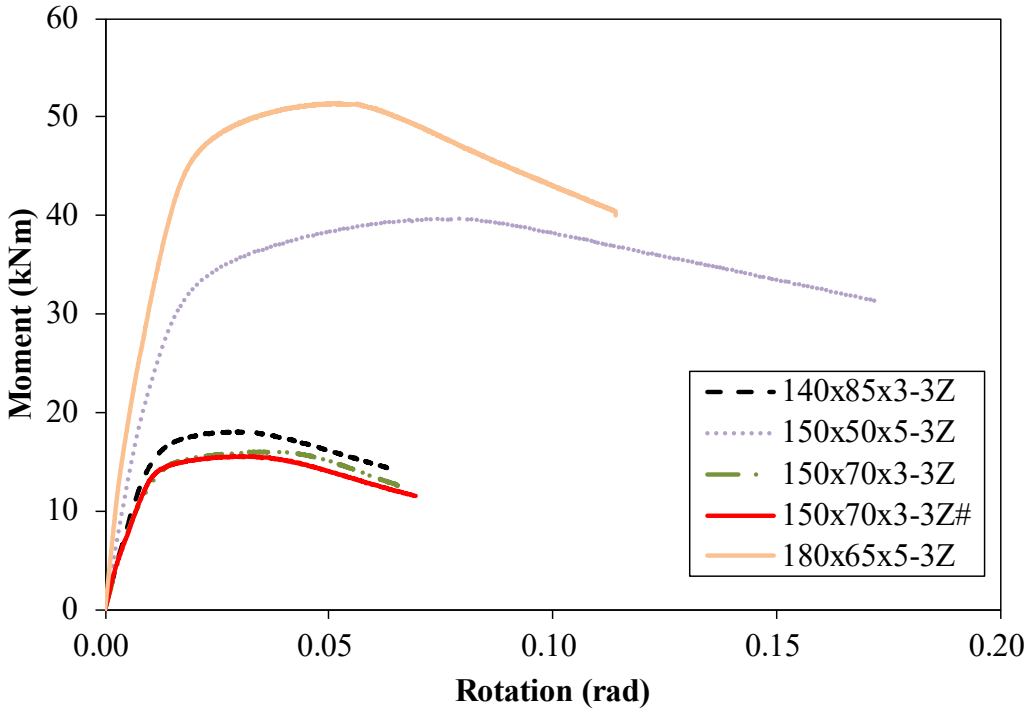

(a) Major axis bending

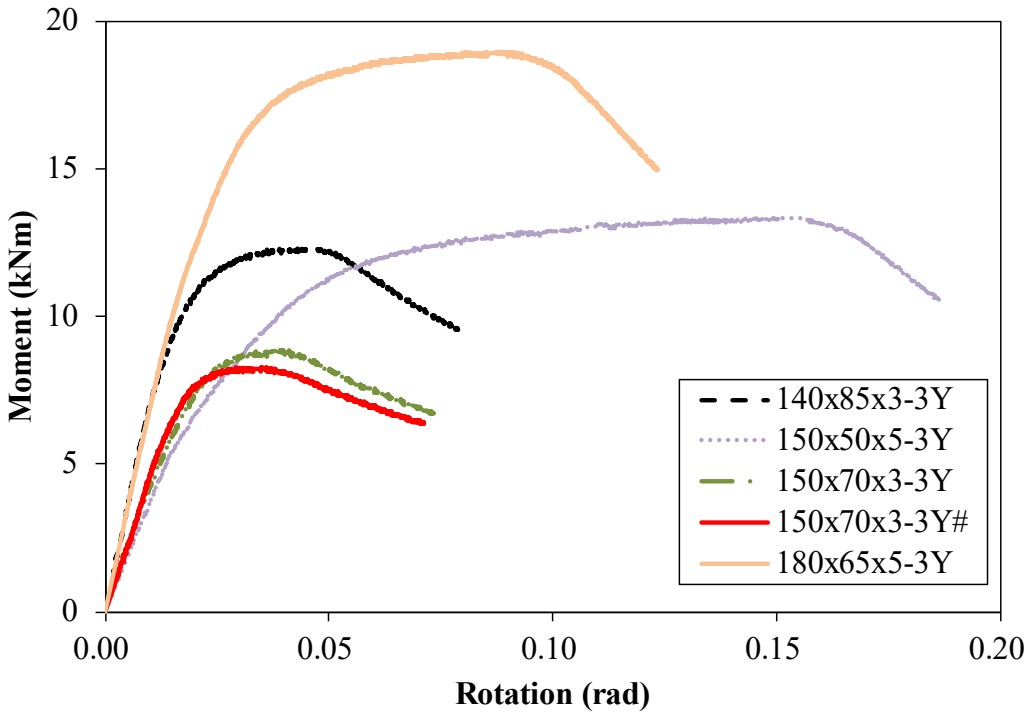

(b) Minor axis bending

Fig. 6. Moment-rotation relationship of EHS beam members subjected to three-point bending

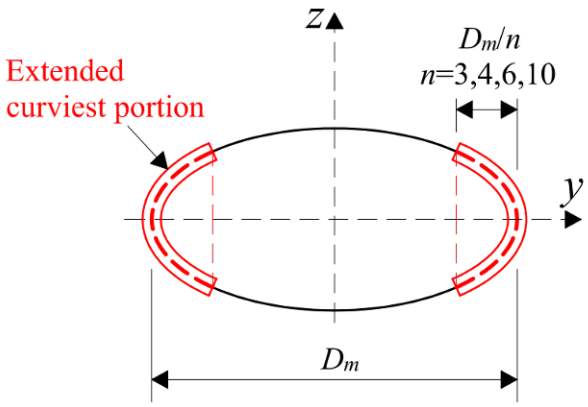

Fig. 7. Extension of strength enhancement at the curviest portion of EHS [17]

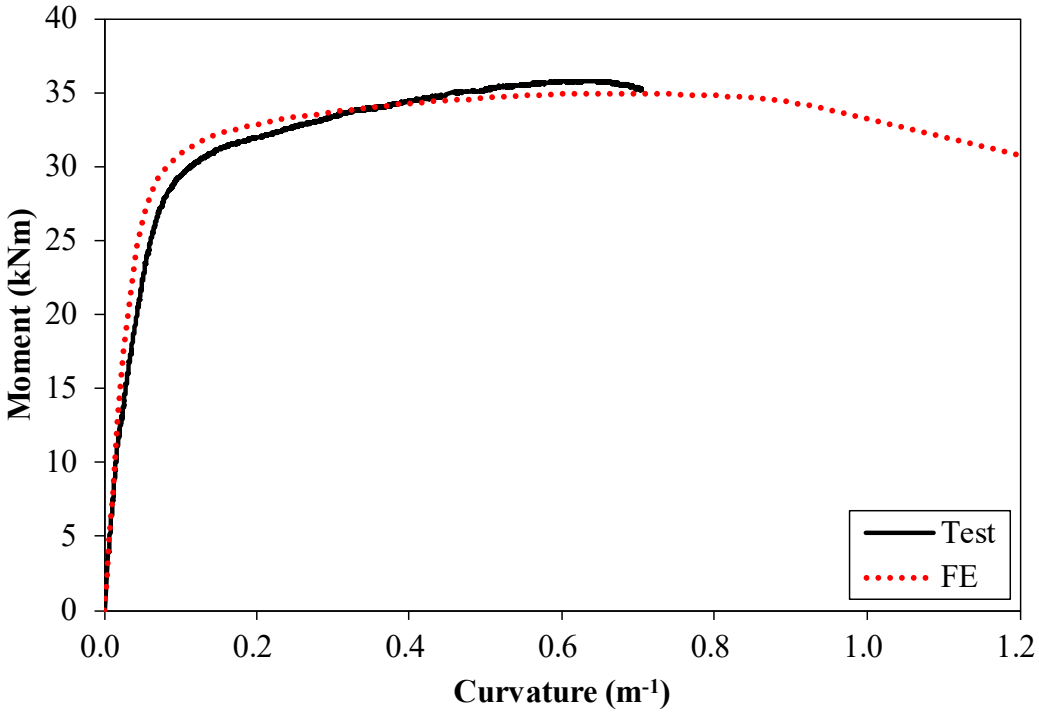

(a) EHS beam 150×50×5-4Z in major axis bending

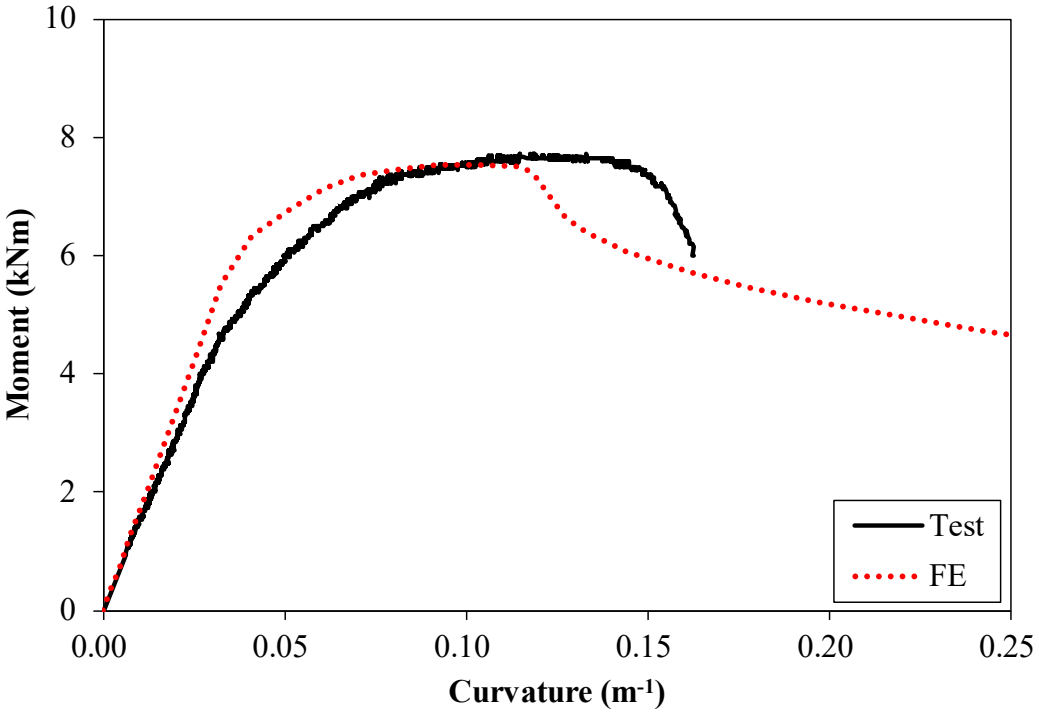

(b) EHS beam 150×70×3-4Y in minor axis bending

Fig. 8. Comparison between experimental and numerical moment-curvature responses of EHS beam specimens

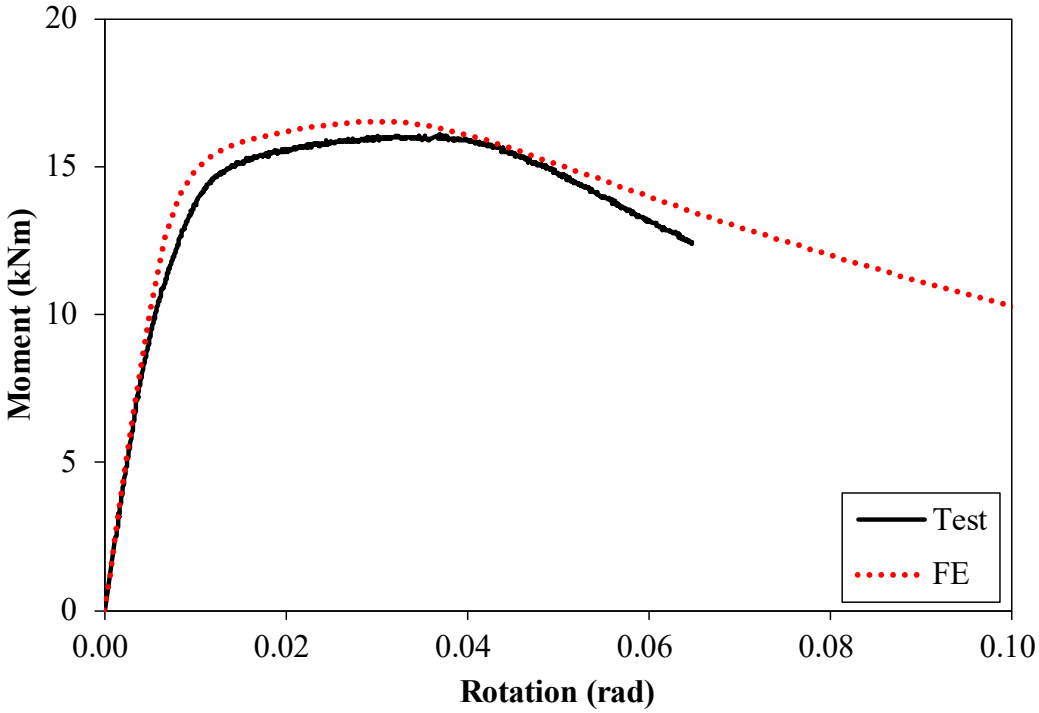

(a) EHS beam 150×70×3-3Z in major axis bending

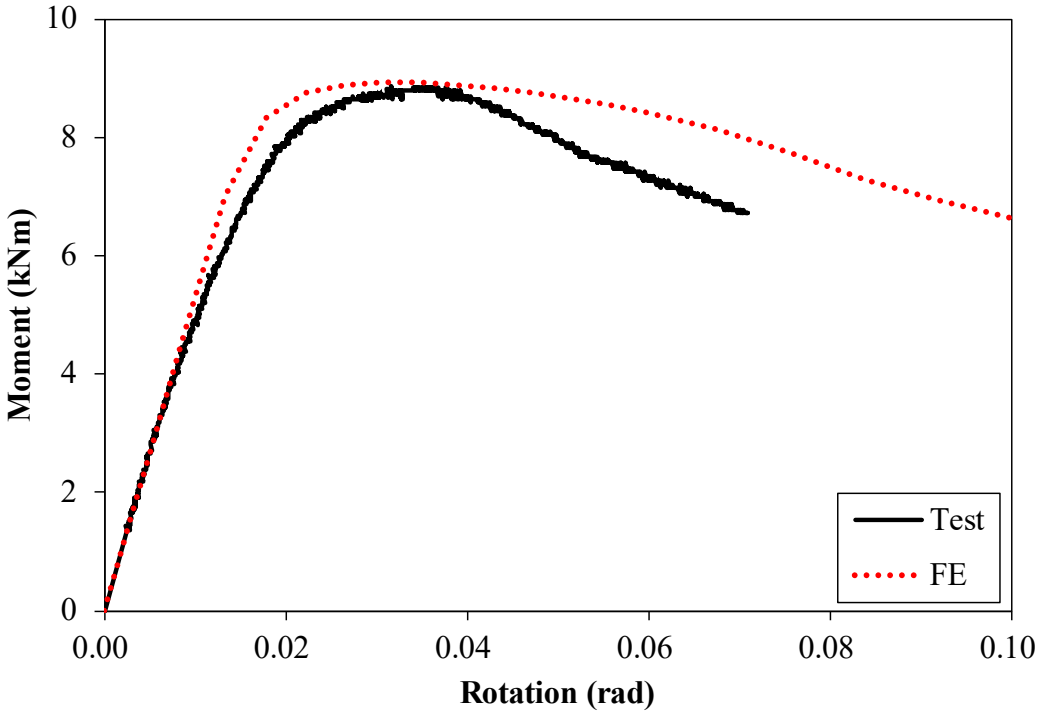

(b) EHS beam 150×70×3-3Y in minor axis bending

Fig. 9. Comparison between experimental and numerical moment-rotation responses of EHS beam specimens

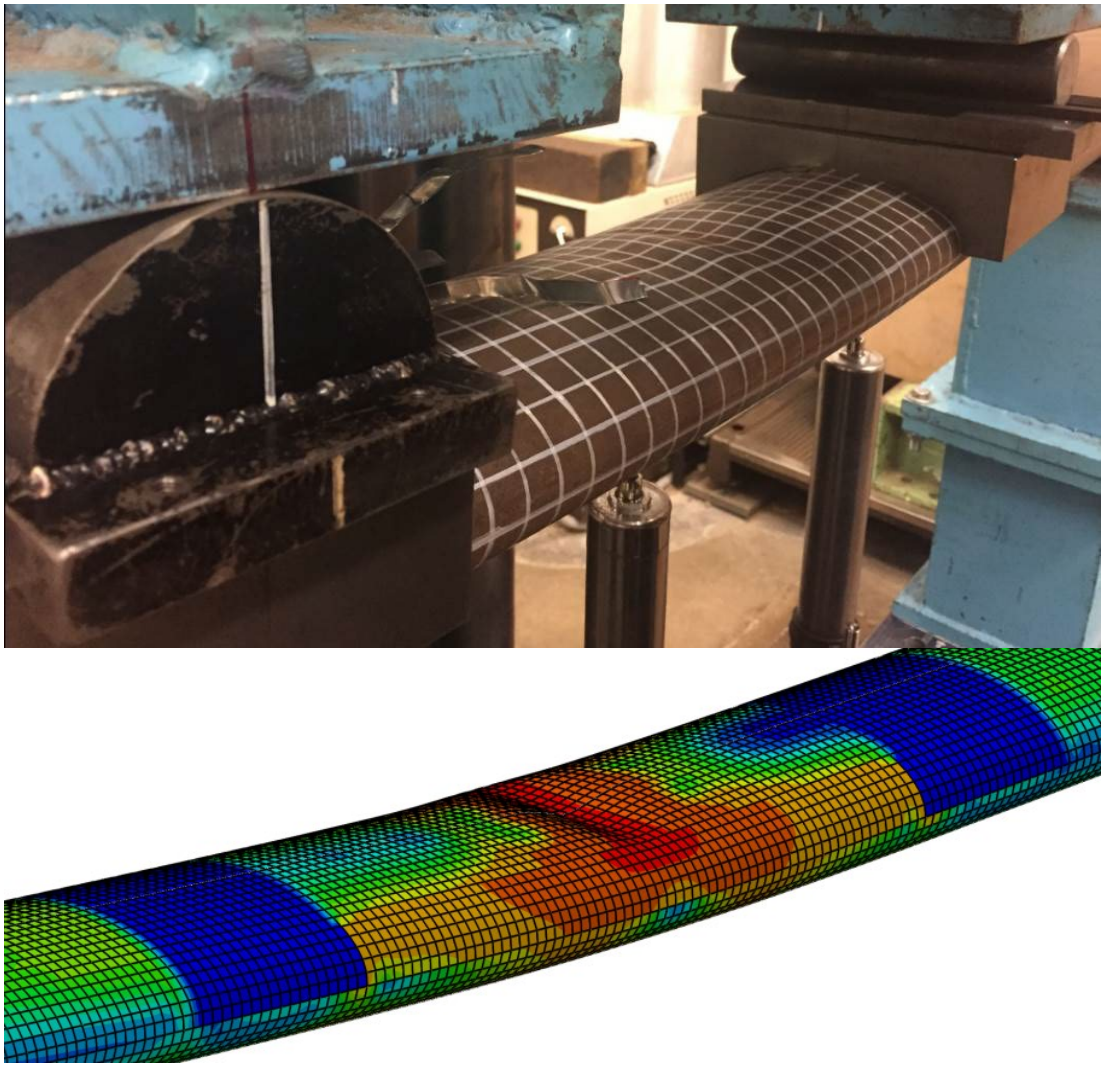

Fig. 10. Comparison between experimental and numerical failure modes for EHS beam 150×70×3-4Y

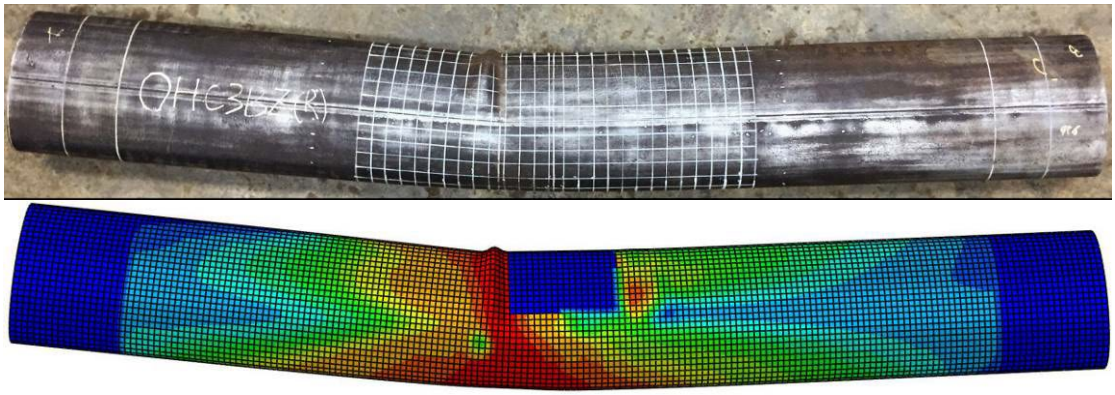

Fig. 11. Comparison between experimental and numerical failure modes of EHS beam 150×70×3-3Z#

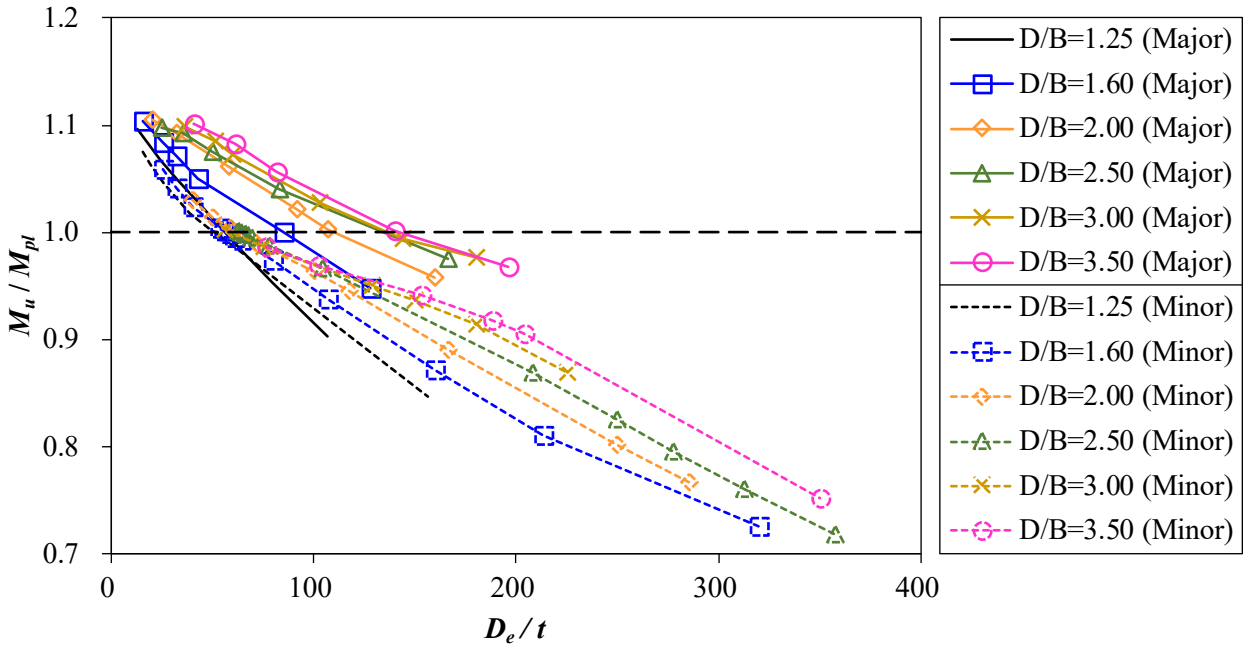

Fig. 12. Effects of different parameters on the moment capacity of EHS beams

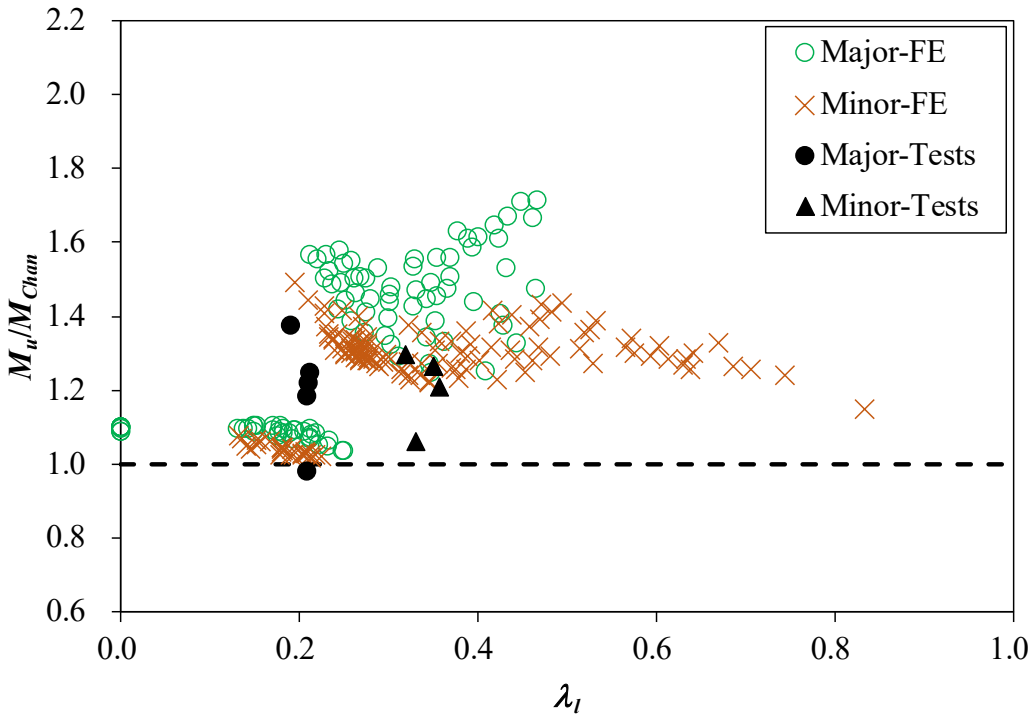

Fig. 13. Comparison of test and FE results of EHS beams with design strengths predicted by the equivalent diameter method

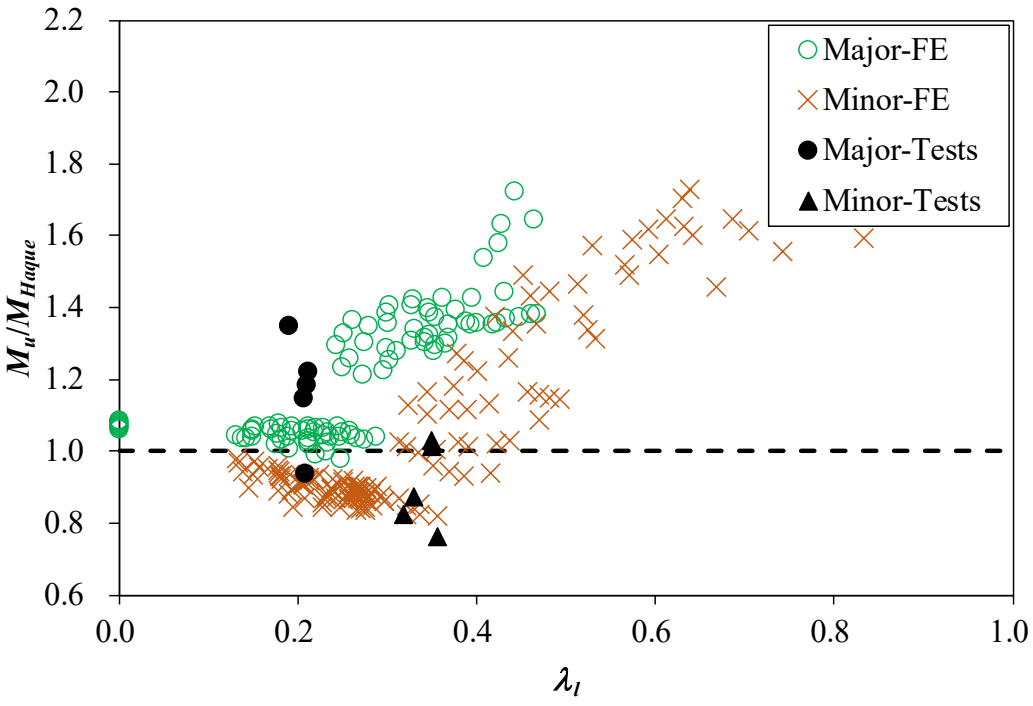

Fig. 14. Comparison of test and FE results of EHS beams with design strengths predicted by the equivalent RHS approach

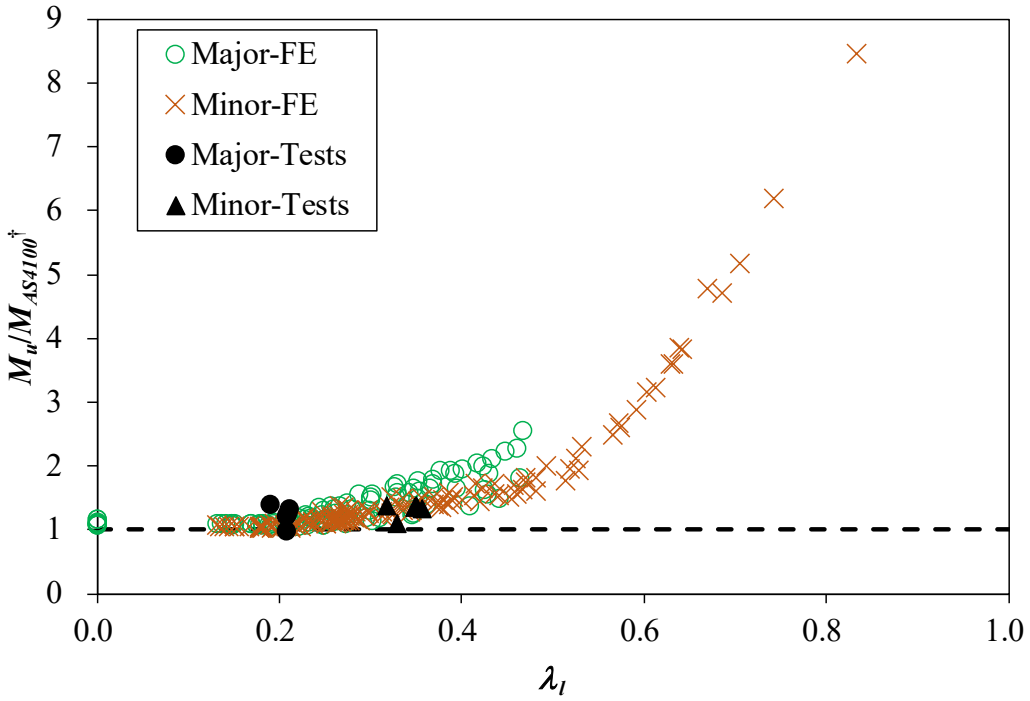

Fig. 15. Comparison of test and FE results of EHS beams with design strengths predicted by the AS4100 [20] using equivalent diameter

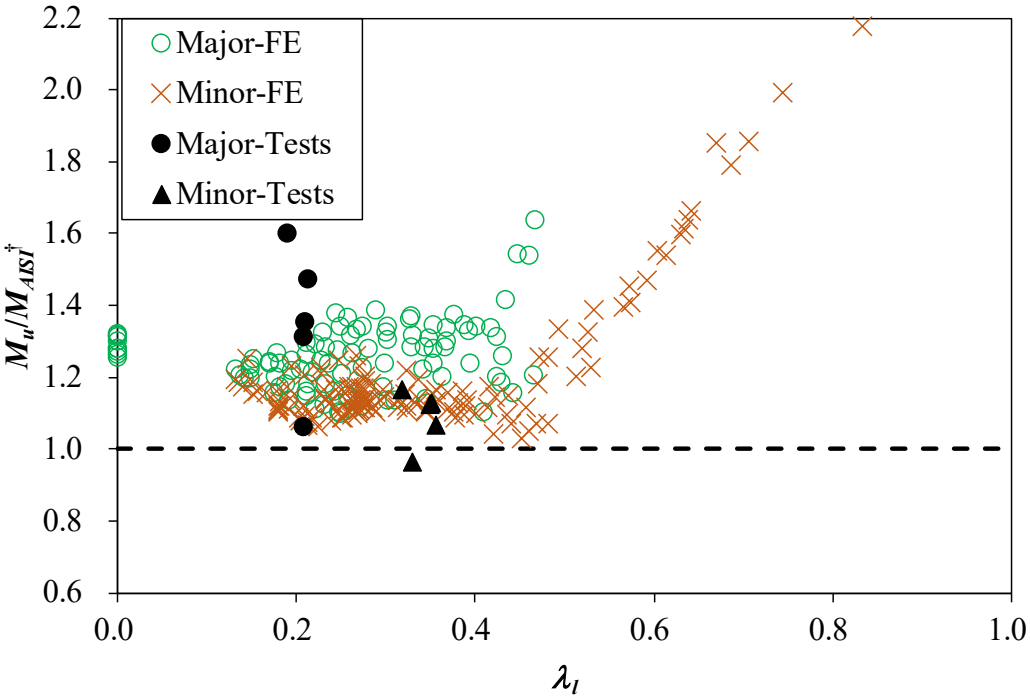

Fig. 16. Comparison of test and FE results of EHS beams with design strengths predicted by the AISI-S100 [18] using equivalent diameter

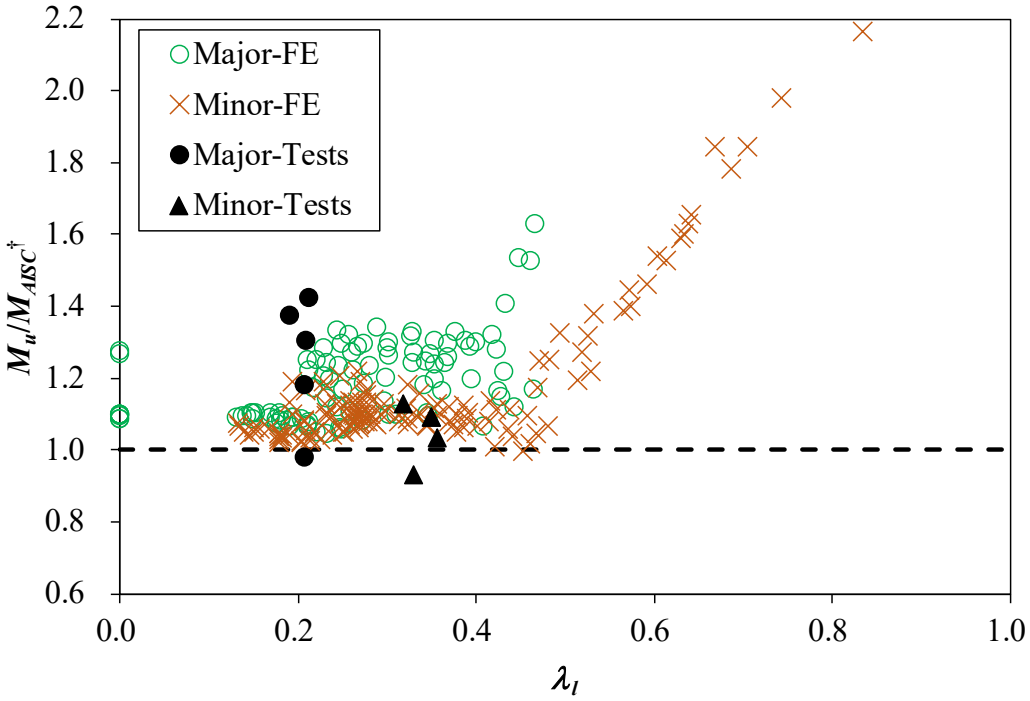

Fig. 17. Comparison of test and FE results of EHS beams with design strengths predicted by the ANSI/AISC360 [19] using equivalent diameter

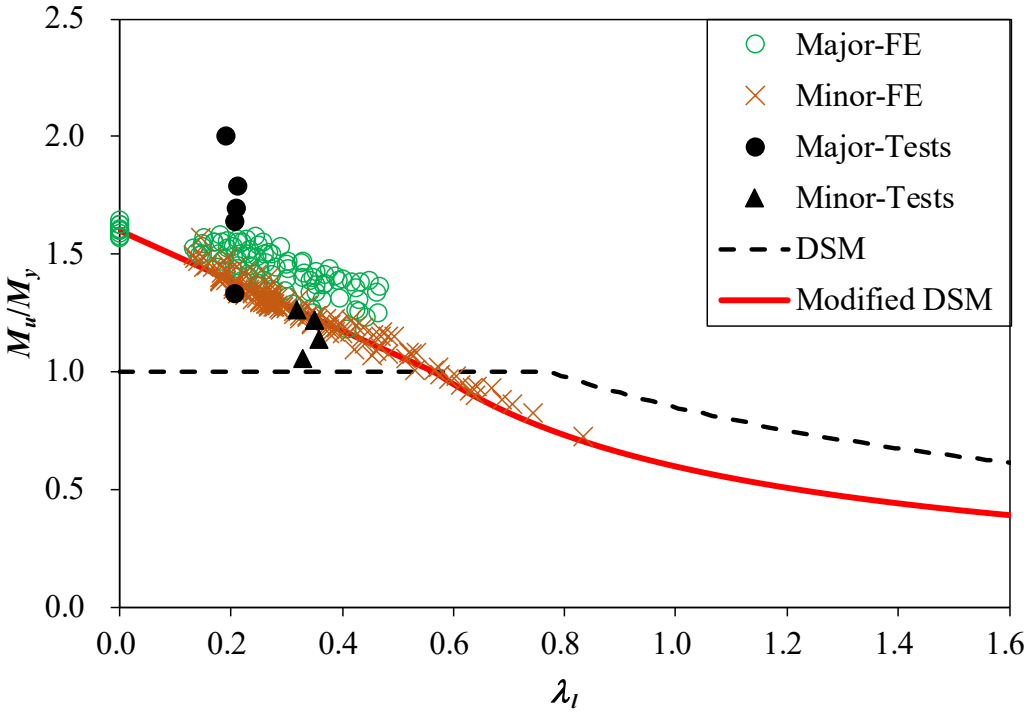

Fig. 18. Comparison of test and FE results of EHS beams with design curves of the existing and modified DSM

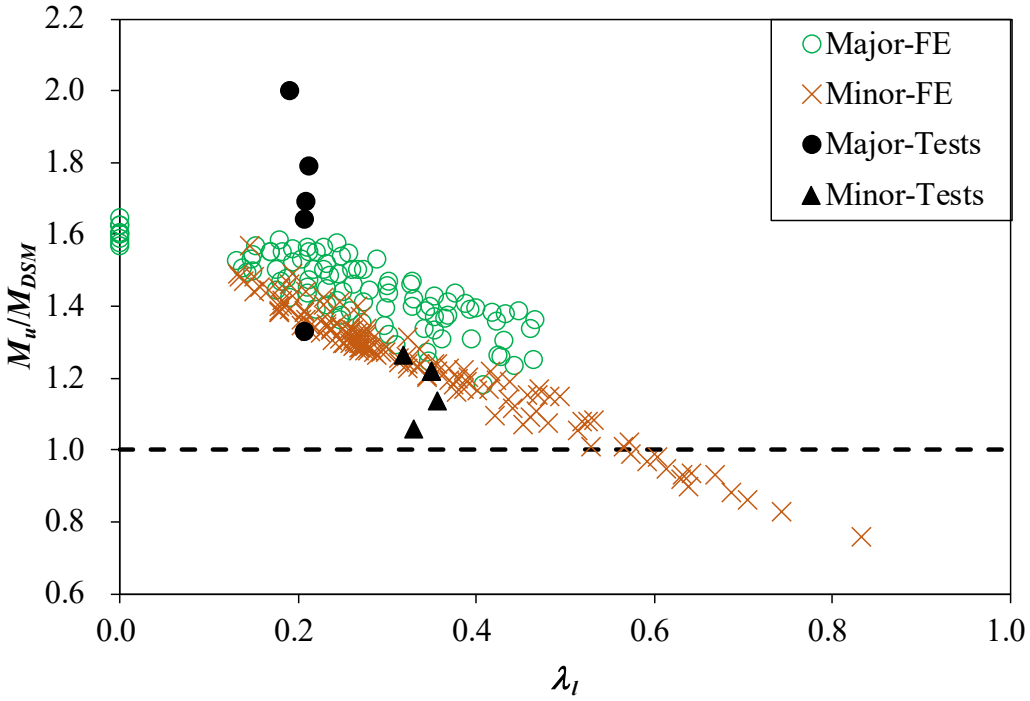

Fig. 19. Comparison of test and FE results of EHS beams with design strengths predicted by the DSM without consideration of inelastic reserve capacity

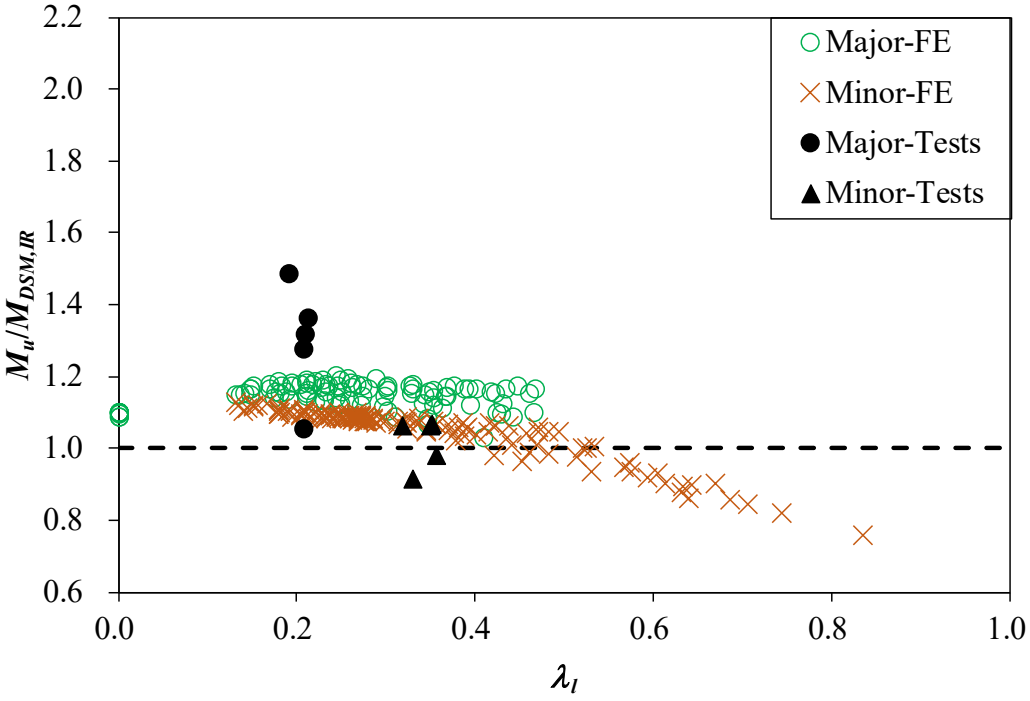

Fig. 20. Comparison of test and FE results of EHS beams with design strengths predicted by the DSM with consideration of inelastic reserve capacity

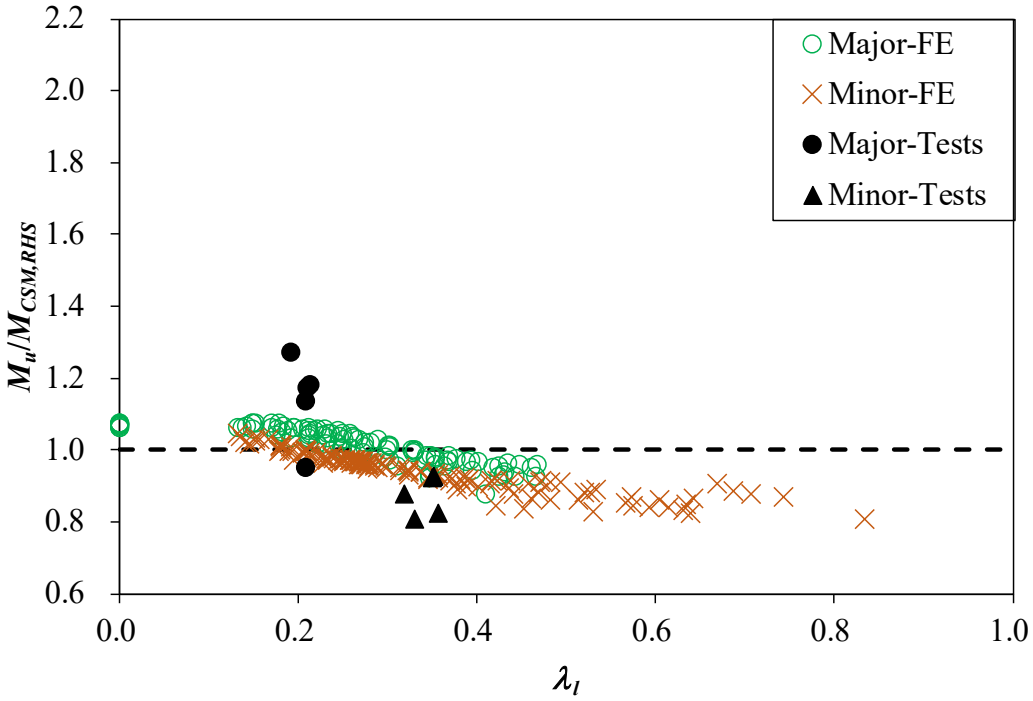

Fig. 21. Comparison of test and FE results of EHS beams with design strengths predicted by the RHS approach of the CSM

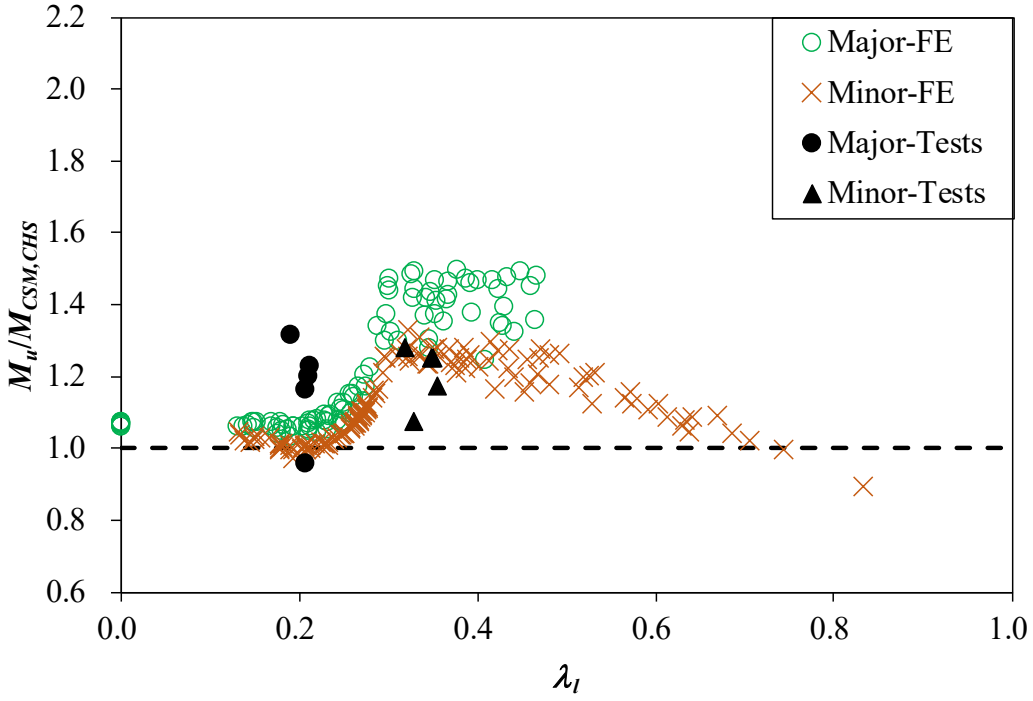

Fig. 22. Comparison of test and FE results of EHS beams with design strengths predicted by the CHS approach of the CSM

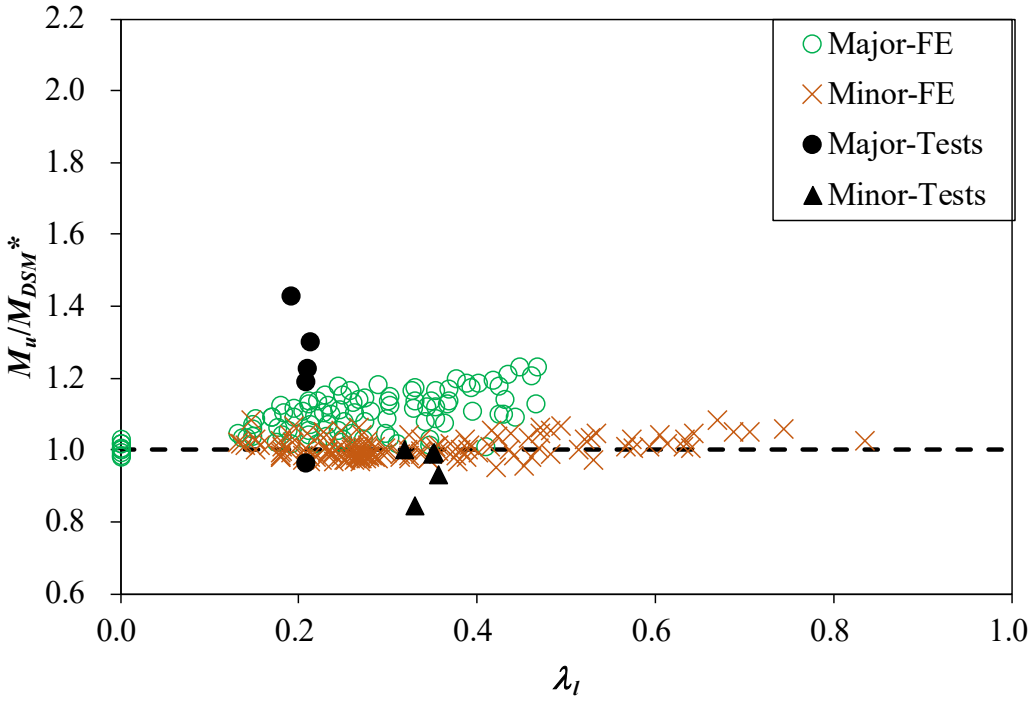

Fig. 23. Comparison of test and FE results of EHS beams with design strengths predicted by the modified DSM

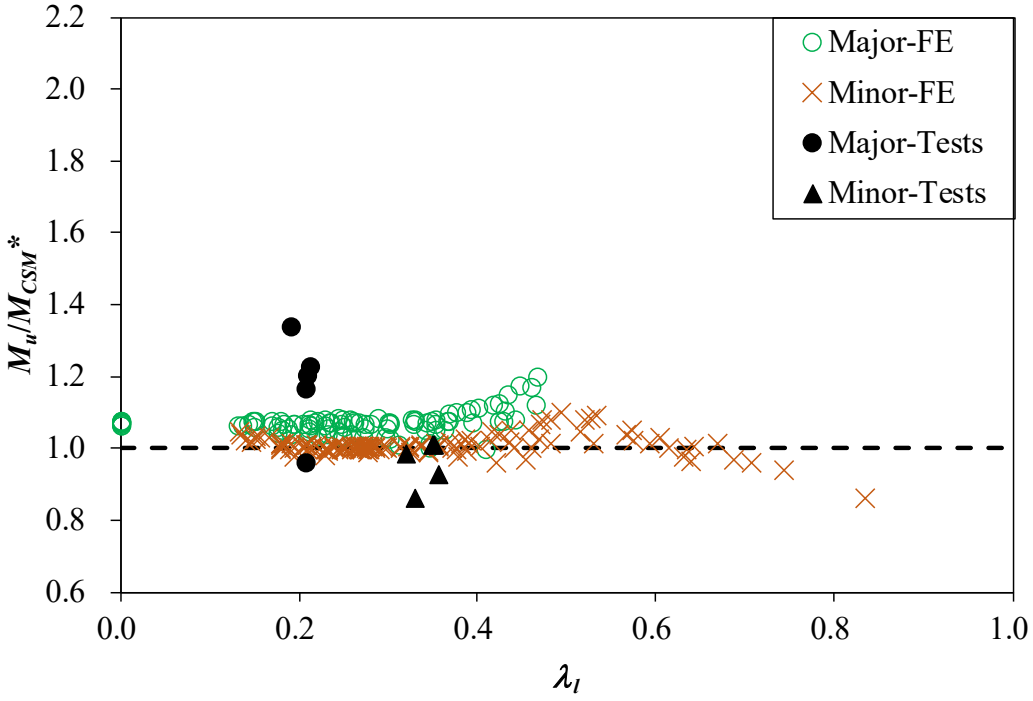

Fig. 24. Comparison of test and FE results of EHS beams with design strengths predicted by the modified CSM

Specimen	Axis of bending	D (mm)	B (mm)	t (mm)	L (mm)
140×85×3-4Z	Major	141.2	87.5	2.91	1610
150×50×5-4Z	Major	149.8	52.0	5.06	1610
150×70×3-4Z	Major	148.5	71.9	2.83	1610
150×70×3-4Z#	Major	148.3	72.4	2.87	1610
180×65×5-4Z	Major	176.4	66.1	4.81	1610
140×85×3-4Y	Minor	141.4	87.6	2.73	1810
150×50×5-4Y	Minor	150.4	51.7	4.98	1810
150×70×3-4Y	Minor	147.8	73.0	2.70	1810
150×70×3-4Y#	Minor	148.6	72.1	2.77	1810
180×65×5-4Y	Minor	176.7	65.1	4.83	1810
140×85×3-3Z	Major	140.7	87.9	2.93	1110
150×50×5-3Z	Major	150.7	50.5	5.02	1110
150×70×3-3Z	Major	148.1	72.6	2.73	1110
150×70×3-3Z#	Major	148.1	72.4	2.71	1110
180×65×5-3Z	Major	176.0	66.7	4.84	1110
140×85×3-3Y	Minor	141.0	87.5	2.96	1310
150×50×5-3Y	Minor	150.4	52.3	5.00	1310
150×70×3-3Y	Minor	148.4	72.7	2.72	1310
150×70×3-3Y#	Minor	148.1	72.6	2.66	1310
180×65×5-3Y	Minor	176.3	65.5	4.83	1310

Table 1. Measured dimensions of the beam specimens

Section	Flattest Portion (TC1)				Curviest Portion (TC2)			
	E (GPa)	$\sigma_{0.2}$ (MPa)	σ_u (MPa)	ε_f (%)	E (GPa)	$\sigma_{0.2}$ (MPa)	σ_u (MPa)	ε_f (%)
140×85×3	208	388	433	14	213	401	458	13
150×50×5	205	410	521	20	213	529	654	12
150×70×3	210	341	392	16	210	340	397	14
180×65×5	200	418	499	19	206	533	635	12

Table 2. Measured material properties obtained from tensile coupon tests [17]

Specimen	Failure mode	$M_{Exp,3}$ (kNm)	Specimen	Failure mode	$M_{Exp,4}$ (kNm)	$\frac{M_{Exp,3}}{M_{Exp,4}}$
140×85×3-3Z	L+Y	18.1	140×85×3-4Z	L+Y	16.0	1.13
150×50×5-3Z	Y	39.7	150×50×5-4Z	Y	35.8	1.11
150×70×3-3Z	L+Y	16.1	150×70×3-4Z	L+Y	16.9	0.95
150×70×3-3Z#	L+Y	15.6	150×70×3-4Z#	L+Y	16.6	0.94
180×65×5-3Z	Y	51.4	180×65×5-4Z	Y	45.5	1.13
140×85×3-3Y	L+Y	12.3	140×85×3-4Y	L+Y	9.2	1.34
150×50×5-3Y	Y	13.3	150×50×5-4Y	Y	10.8	1.23
150×70×3-3Y	L+Y	8.9	150×70×3-4Y	L+Y	7.7	1.14
150×70×3-3Y#	L+Y	8.3	150×70×3-4Y#	L+Y	7.8	1.06
180×65×5-3Y	Y	18.95	180×65×5-4Y	Y	15.1	1.26
					Mean	1.13
					COV	0.112

Table 3. Summary of test results and comparison

Specimen	M_{Exp}/M_{FE} Material division (With no imperfection)				M_{Exp}/M_{FE} Local imperfection (with $D_m/6$ material division)			
	$D_m/3$	$D_m/4$	$D_m/6$	$D_m/10$	$t/3$	$t/10$	$t/50$	$t/100$
140×85×3-4Z	0.90	0.91	0.92	0.93	0.99	0.94	**0.92**	0.92
150×50×5-4Z	0.95	0.98	1.02	1.07	1.09	1.04	**1.02**	1.02
150×70×3-4Z	1.16	1.16	1.16	1.17	1.17	1.16	**1.16**	1.16
150×70×3-4Z#	1.12	1.12	1.13	1.13	1.13	1.13	**1.13**	1.13
180×65×5-4Z	0.90	0.92	0.97	1.02	0.97	0.97	**0.97**	0.97
140×85×3-4Y	0.83	0.84	0.85	0.86	0.97	0.89	**0.86**	0.86
150×50×5-4Y	0.83	0.88	0.93	0.96	1.03	0.95	**0.93**	0.93
150×70×3-4Y	1.01	1.01	1.02	1.02	1.18	1.06	**1.02**	1.02
150×70×3-4Y#	1.01	1.01	1.01	1.01	1.17	1.05	**1.02**	1.02
180×65×5-4Y	0.77	0.82	0.86	0.89	0.98	0.89	**0.87**	0.86
140×85×3-3Z	0.86	0.87	0.87	0.88	0.88	0.87	**0.87**	0.87
150×50×5-3Z	0.86	0.89	0.92	0.96	0.92	0.92	**0.92**	0.92
150×70×3-3Z	0.97	0.97	0.97	0.98	0.98	0.97	**0.97**	0.97
150×70×3-3Z#	0.95	0.95	0.95	0.96	0.96	0.95	**0.95**	0.95
180×65×5-3Z	0.84	0.87	0.90	0.94	0.91	0.90	**0.90**	0.90
140×85×3-3Y	0.88	0.89	0.90	0.91	0.91	0.90	**0.90**	0.90
150×50×5-3Y	0.80	0.84	0.89	0.92	0.89	0.89	**0.89**	0.89
150×70×3-3Y	0.98	0.99	0.99	0.99	1.00	0.99	**0.99**	0.99
150×70×3-3Y#	0.94	0.95	0.95	0.95	0.96	0.95	**0.95**	0.95
180×65×5-3Y	0.78	0.83	0.88	0.92	0.88	0.88	**0.88**	0.88
Mean	0.92	0.94	0.96	0.97	1.00	0.97	**0.96**	0.96
COV	0.113	0.099	0.087	0.081	0.098	0.087	**0.087**	0.087

Table 4. Summary of sensitivity study

Specimen	M_{FE} (kNm)	Specimen	M_{FE} (kNm)
500×250×16-Z	1093.6	500×200×5-Y	128.7
500×250×10-Z	692.2	500×200×4.5-Y	112.0
500×250×8.5-Z	587.9	500×200×4-Y	95.6
500×250×6-Z	411.0	500×200×3.5-Y	79.3
500×250×4-Z	266.4	400×250×25-Y	763.1
500×250×3.5-Z	230.7	400×250×20-Y	622.6
500×200×16-Z	1007.4	400×250×16-Y	504.3
500×200×12-Z	763.5	400×250×12-Y	381.9
500×200×8-Z	507.1	400×250×11.5-Y	366.3
500×200×4-Z	245.6	400×250×11-Y	350.5
500×200×3.5-Z	212.3	400×250×10.5-Y	334.7
400×250×16-Z	761.1	400×250×10-Y	318.8
400×250×10-Z	484.5	400×250×8-Y	254.0
400×250×8-Z	387.3	400×250×6-Y	186.0
400×250×6-Z	288.0	400×250×4-Y	116.9
400×250×3-Z	139.6	400×250×3-Y	82.0
400×250×2-Z	88.8	400×250×2-Y	49.3
400×200×16-Z	687.2	400×200×20-Y	463.1
400×200×10-Z	440.9	400×200×16-Y	377.4
400×200×5.5-Z	242.2	400×200×14-Y	332.9
400×200×3.5-Z	150.1	400×200×13.5-Y	321.7
400×200×3-Z	126.7	400×200×13-Y	310.3
400×200×2-Z	81.2	400×200×12.5-Y	298.9
350×200×14-Z	487.9	400×200×12-Y	287.4
350×200×7-Z	250.2	400×200×10-Y	240.4
350×200×5-Z	177.9	400×200×5.5-Y	127.7
350×200×3.5-Z	122.3	400×200×4-Y	87.6
350×200×2-Z	66.7	400×200×3-Y	61.1
350×200×1.5-Z	48.0	350×200×20-Y	417.3
350×100×12-Z	334.7	350×200×16-Y	340.0

350×100×8-Z	226.1	350×200×12-Y	259.1
350×100×6-Z	168.0	350×200×7-Y	151.9
350×100×3.5-Z	94.6	350×200×5-Y	105.6
350×100×2.5-Z	65.8	350×200×3.5-Y	69.7
325×100×10-Z	246.3	350×200×2-Y	34.6
325×100×6.5-Z	160.8	350×100×16-Y	138.7
325×100×4-Z	96.7	350×100×12-Y	108.5
325×100×2.5-Z	57.8	350×100×8-Y	74.4
325×100×2-Z	45.8	350×100×6.5-Y	60.2
300×200×8-Z	224.1	350×100×6-Y	55.2
300×200×6-Z	168.0	350×100×3.5-Y	27.7
300×200×4-Z	110.6	325×100×16-Y	129.9
300×200×2-Z	53.4	325×100×14-Y	116.2
300×200×1.5-Z	38.7	325×100×10-Y	86.3
300×100×16-Z	323.5	325×100×6.5-Y	57.0
300×100×10-Z	212.8	325×100×5.5-Y	47.7
300×100×7-Z	151.0	325×100×2.5-Y	16.8
300×100×6-Z	129.2	325×100×2-Y	11.9
300×100×3.5-Z	73.7	300×200×20-Y	370.2
300×100×2.5-Z	51.4	300×200×16-Y	302.9
300×100×2-Z	40.6	300×200×12-Y	231.0
275×100×6.5-Z	120.7	300×200×8-Y	155.6
275×100×4.5-Z	83.1	300×200×6-Y	116.2
275×100×3.5-Z	64.0	300×200×4-Y	74.9
275×100×2-Z	35.4	300×100×16-Y	120.8
275×100×1.5-Z	25.7	300×100×12-Y	94.9
270×120×8-Z	152.0	300×100×7-Y	57.5
270×120×6.5-Z	124.4	300×100×6-Y	49.3
270×120×4.5-Z	86.2	300×100×5-Y	40.7
270×120×2.5-Z	46.9	300×100×4-Y	31.4
270×120×2-Z	36.6	275×100×16-Y	111.8
250×200×12-Z	249.8	275×100×10-Y	74.9
250×200×6.5-Z	138.4	275×100×6.5-Y	49.9
250×200×5-Z	106.2	275×100×4.5-Y	34.1
250×200×4-Z	84.3	275×100×3.5-Y	25.4
250×200×2.5-Z	50.9	275×100×2-Y	12.1
250×200×2-Z	39.6	270×120×16-Y	140.4
250×200×1.5-Z	28.3	270×120×12-Y	109.3
250×100×10-Z	153.3	270×120×8-Y	75.1
250×100×7-Z	110.1	270×120×6.5-Y	61.4
250×100×5-Z	79.0	270×120×4.5-Y	42.0
250×100×3-Z	46.8	270×120×2.5-Y	20.9
250×100×1.5-Z	22.3	270×120×2-Y	15.7
210×120×12-Z	143.9	250×200×20-Y	321.9
210×120×6-Z	76.2	250×200×16-Y	265.1
210×120×3.5-Z	44.8	250×200×12-Y	203.4
210×120×2.5-Z	31.7	250×200×8-Y	137.2
210×120×1.5-Z	18.3	250×200×6.5-Y	111.7
200×150×10-Z	127.4	250×200×6-Y	103.0
200×150×6-Z	78.5	250×200×5-Y	85.4
200×150×3-Z	39.2	250×200×4-Y	67.4
200×150×2.5-Z	32.4	250×200×2-Y	30.2
200×150×2-Z	25.5	250×100×16-Y	102.9
200×150×1.5-Z	18.6	250×100×12-Y	81.0
200×150×1-Z	12.1	250×100×11-Y	75.1
180×80×8-Z	65.0	250×100×10.5-Y	72.1
180×80×6-Z	50.0	250×100×10-Y	69.0
180×80×3.5-Z	29.7	250×100×7-Y	49.6
180×80×2-Z	16.8	250×100×5-Y	35.6
180×80×1.5-Z	12.4	210×120×16-Y	113.9
150×100×8-Z	53.1	210×120×12-Y	89.2
150×100×6-Z	40.9	210×120×10-Y	75.7
150×100×2.5-Z	17.3	210×120×6-Y	46.7
150×100×1.5-Z	10.2	210×120×3.5-Y	27.0
150×50×8-Z	40.0	210×120×2.5-Y	18.4

150×50×6-Z	31.1	200×150×16-Y	149.4
150×50×4-Z	21.3	200×150×10-Y	98.6
150×50×2.5-Z	13.3	200×150×8-Y	79.8
150×50×1.5-Z	7.8	200×150×6-Y	60.3
500×250×25-Y	907.1	200×150×5.5-Y	55.3
500×250×20-Y	738.6	200×150×3-Y	29.4
500×250×17-Y	634.4	200×150×2.5-Y	23.9
500×250×16.5-Y	616.0	200×150×2-Y	18.2
500×250×16-Y	598.1	180×80×16-Y	56.4
500×250×14-Y	525.6	180×80×12-Y	45.4
500×250×10-Y	375.2	180×80×8-Y	32.2
500×250×8.5-Y	315.8	180×80×6-Y	24.8
500×250×6-Y	213.3	180×80×3.5-Y	14.6
500×250×4-Y	129.7	150×100×12-Y	52.8
500×250×3.5-Y	109.0	150×100×8-Y	37.3
500×200×20-Y	556.4	150×100×6-Y	28.6
500×200×19.5-Y	543.8	150×100×4-Y	19.3
500×200×19-Y	531.2	150×100×2.5-Y	11.9
500×200×18.5-Y	518.4	150×50×10-Y	17.6
500×200×18-Y	505.5	150×50×8-Y	14.9
500×200×16-Y	453.0	150×50×6-Y	11.7
500×200×12-Y	343.0	150×50×4-Y	8.1
500×200×6-Y	161.4		

Table 5. Parametric study on cold-formed steel EHS beams in both major and minor axes bending

Number of		$\frac{M_u}{M_{Chan}}$	$\frac{M_u}{M_{Haque}}$	$\frac{M_u}{M_{AS4100}{}^{\dagger}}$	$\frac{M_u}{M_{AISI}{}^{\dagger}}$	$\frac{M_u}{M_{AISC}{}^{\dagger}}$	$\frac{M_u}{M_{DSM}}$	$\frac{M_u}{M_{DSM,IR}}$	$\frac{M_u}{M_{CSM,RHS}}$	$\frac{M_u}{M_{CSM,CHS}}$	$\frac{M_u}{M_{DSM}{}^{*}}$	$\frac{M_u}{M_{CSM}{}^{*}}$
Test:10	FE:235											
Major: 104	Mean	1.32	1.21	1.36	1.27	1.20	1.46	1.15	1.02	1.22	**1.10**	**1.08**
	COV	0.159	0.146	0.241	0.081	0.098	0.084	0.048	0.057	0.136	**0.067**	**0.044**
Minor: 141	Mean	1.26	1.05	1.59	1.20	1.16	1.25	1.05	0.94	1.12	**1.00**	**1.01**
	COV	0.095	0.237	0.647	0.155	0.169	0.124	0.066	0.058	0.091	**0.031**	**0.030**
ALL: 245	Mean	1.28	1.11	1.49	1.23	1.18	1.34	1.10	0.98	1.16	**1.05**	**1.04**
	COV	0.130	0.210	0.547	0.130	0.143	0.132	0.074	0.070	0.121	**0.069**	**0.049**
	ϕ	1.00	1.00	0.90	0.95	0.90	0.90	0.90	1.00	1.00	**0.90**	**0.90**
	β	2.67	1.84	1.61	2.84	2.81	3.34	2.85	1.82	2.34	**2.68**	**2.54**

† Nominal design strengths predicted by adopting the equivalent diameter proposed by Chan *et al.* [14]

***** Modified design methods

Table 6. Comparison of cold-formed steel EHS beam test and FE results with predicted strengths